Available online at www.sciencedirect.com
ScienceDirect
Remote Sensing of Environment 107 (2007) 90–108
Remote Sensing of Environment
www.elsevier.com/locate/rse

Simultaneous retrieval of aerosol and surface properties from a combination of AERONET and satellite data

Alexander Sinyuk [a,b,*], Oleg Dubovik [a,1], Brent Holben [a], Tom F. Eck [a,c], Francois-Marie Breon [d], John Martonchik [e], Ralph Kahn [e], David J. Diner [e], Eric F. Vermote [f], Jean-Claude Roger [a,f,g,2], Tatyana Lapyonok [a,b], Ilya Slutsker [a,b]

[a] *Laboratory for Terrestrial Physics, NASA Goddard Spaceflight Center, Greenbelt, MD, USA*
[b] *Science Systems and Applications, Inc., Lanham, MD, USA*
[c] *GEST Center, University of Maryland, Baltimore County, Baltimore, MD,USA*
[d] *Laboratoire des Sciences du Climat et de l'Environnement, Gif Sur Yvette, France*
[e] *Jet Propulsion Laboratory, California Institute of Technology, Pasadena, CA, USA*
[f] *University of Maryland, College Park, MD, USA*
[g] *ELICO, Université du Littoral Côte d'Opale, France*

Received 7 April 2006; received in revised form 23 June 2006; accepted 16 July 2006

Abstract

We present a method for simultaneously retrieving aerosol and surface parameters from ground-based and satellite observations collocated in space and time. We show that a combination of down and up-looking observations provides sufficient measurement constraints for characterizing both aerosol and surface properties with minimal assumptions. In order to employ this concept in AERONET processing, the standard inverse algorithm [Dubovik, O. & King, M. D. (2000), A flexible inversion algorithm for retrieval of aerosol optical properties from sun and sky radiance measurements. *Journal of Geophysical Research*, 105, 20673–20696] has been modified to retrieve surface reflectance in addition to aerosol parameters when co-incident satellite measurements are available.

The method was applied to observations of smoke and desert dust over the Mongu (Zambia) and Solar Village (Saudi Arabia) AERONET sites respectively. The AERONET data were complemented by available observations from the MISR, MODIS, and POLDER-2 satellite sensors. The retrieved bidirectional reflectance factor (BRF) and surface albedo comparison shows good agreement between results obtained using observations from different satellites.

The robustness of the method is tested by analyzing surface albedo time series retrieved during periods of high aerosol optical depth variability and low seasonal changes in surface reflectance. The analysis shows that the performance of retrieval algorithm is stable under different aerosol loadings. It is shown that much of the observed surface albedo temporal variability could be attributed mostly to the combined uncertainty in satellite radiometric calibration and aerosol vertical distribution for Mongu and to differences in satellite angular sampling on different days for Solar Village.

The sensitivity of surface retrievals to assumptions on aerosol vertical distribution and aerosol particle shape are analyzed. It is found that the maximum error in retrieved surface albedo at 0.44 μm is 0.035 for aerosol optical depth 0.85 at 0.44 μm. For aerosol optical depths lower than ~0.7 the error in retrieved surface albedo is less than 0.02. Analysis of particle shape assumptions on surface retrievals showed that aerosol particle non-sphericity significantly affects the angular shape of BRF, but not the surface albedo.

Finally, the sensitivity of AERONET aerosol retrievals to uncertainty in assumed surface reflectance is analyzed by comparing aerosol retrievals obtained with different surface assumptions. It is found that the uncertainty in surface reflectance model employed in the version 1 AERONET operational algorithm is larger than was previously assumed in [Dubovik, O., Smirnov, A., Holben, B. N., King, M. D., Kaufman, Y. J., Eck, T. F., & Slutsker, I. (2000), Accuracy assessment of aerosol optical properties retrieved from AERONET sun and sky radiance measurements. *Journal of Geophysical Research*, 105, 9791–9806] and may have more significant effect on the retrieved aerosol properties than was documented in that work. In particular, larger errors were encountered for the real part of the refractive index (~0.05–0.07 increase) and maximum of the particle size

* Corresponding author. Laboratory for Terrestrial Physics, NASA Goddard Spaceflight Center, Greenbelt, MD, USA.
E-mail address: asiniuk@ltpmail.gsfc.nasa.gov (A. Sinyuk).
[1] Now at Laboratoire d'Optique Atmosphe´rique, Universite´ de Lille 1/CNRS, Villeneuve d'Ascq, France.
[2] Now at OPGC / LAMP Universite Blaise Pascale 24, Avenue des Landais 63177 AUBIÈRE Cedex, France.

doi:10.1016/j.rse.2006.07.022

distribution (~20% decrease) retrievals for the Mongu case, when the aerosol optical depth was relatively small (~0.4 at 0.44 μm). The retrieved single scattering albedo uncertainties were within the error bars (0.03) estimated in [Dubovik, O., Smirnov, A., Holben, B. N., King, M. D., Kaufman, Y. J., Eck, T. F., & Slutsker, I. (2000), Accuracy assessment of aerosol optical properties retrieved from AERONET sun and sky radiance measurements. *Journal of Geophysical Research*, 105, 9791–9806], with the exception of the 0.44 μm retrievals for the desert dust case when they increased by ~0.09 and 0.07 for low and high aerosol loadings respectively.

Keywords: Surface reflectance; Aerosol properties; AERONET; MISR; MODIS; POLDER

1. Introduction

Detailed information on aerosol optical properties is important for understanding aerosol radiative forcing, and impact on climate change (e.g. Charlson et al., 1992; Hansen et al., 1997, 2000; Intergovernmental Panel on Climate Change (IPCC), 2001; Ramanathan et al., 2001; Tegen et al., 1996). Due to their high temporal and spatial variability, atmospheric aerosol monitoring presents a difficult task, and thus significant efforts have been made to improve aerosol characterization by using in situ measurements (e. g. Anderson et al., 2003; Haywood et al., 2003; Reid et al., 1998), ground-based remote sensing (e. g. Holben et al., 2001), satellite observations (e. g. Kaufman et al., 2002a; King et al., 1999), and aerosol transport modeling (e. g. Chin et al., 2002; Ginoux et al., 2001; Tegen et al., 1997).

Satellite remote sensing is an efficient way to monitor aerosol properties on a global scale. Today satellite sensors perform diverse observations of up-welling radiation reflected by the earth–atmosphere system including multi-wavelength, multi-angle, and polarimetric measurements (e. g. King et al., 1999). In general, it is difficult to uniquely derive the complete set of aerosol parameters (particle size distribution, aerosol loading, complex refractive index, and shape) from satellite measurements alone, and a number of additional assumptions are required to constrain some of the aerosol properties. For example, satellite aerosol retrieval algorithms commonly rely on a pre-selected set of aerosol models and choose a model or mixture of candidate models based on the best fit of the measurements to the radiative transfer calculations (e. g. Kaufman et al., 1997a) or define a solution space that includes all mixtures in the set that meet the acceptance criteria (Kahn et al., 2001; Martonchik et al., 1998). Once the best-fit model or space is identified, it is used as a basis for providing a set of integral aerosol characteristics such as optical depth coupled with effective size (e. g. Remer et al., 2002) and/or aerosol absorption (e. g. Kahn et al., 2005; Torres et al., 2005). However, the scientific community anticipates that future satellite missions equipped with higher spectral and angular coverage of multi-angle and polarimetric capabilities will provide yet more detailed aerosol characterization (Mishchenko et al., 2004).

Both surface reflection and aerosol backscattering affect the top-of-atmosphere radiances measured by satellites. Therefore the main challenge in satellite aerosol retrieval is to separate the contributions from the surface and atmosphere. Traditionally aerosol retrieval algorithms rely on measurement scenarios corresponding to low surface reflectivity. For example, the effect of uncertainty in surface properties is less important in satellite retrievals over ocean (excluding glint region) in visible and in near-IR (e.g. Kaufman et al., 1997b; Remer et al., 2005; Tanre et al., 1997) and over land in near-UV portions of the spectrum (e. g. Torres et al., 1998). Also, some surface types, such as dense vegetation have low reflectance in the blue and red regions (Kaufman & Sendra, 1988). In these cases the retrievals either assume the surface reflectance using reflectance databases (e. g. Hsu et al., 2004; Torres et al., 1998) or rely on surface reflectance correlation between the visible and middle-IR spectral regions (Kaufman et al., 2002b). Utilization of satellite observations in the visible and near-IR over arid or unvegetated surfaces presents a more challenging task because the satellite signal is dominated by a large surface contribution (Kaufman et al., 1997a). Multi-angle and polarimetric satellite observations allow better characterization of aerosol over these types of surfaces. For example, the Multi-angle Imaging Spectroradiometer (MISR) algorithm distinguishes between aerosol and surface contributions based on differences in surface and atmosphere angular reflectance signatures (Diner et al., 2005). The polarization and Directionality of the Earth's Reflectances (POLDER) retrieval relies on the differences in polarization properties of atmospheric and surface signals (Deuze et al., 2001).

The approach of the present study is to combine satellite observations with collocated ground-based measurements. Such a combination of data enables the separation of aerosol and surface signals. Indeed, the reflected signal is sensitive to both surface reflectance and aerosol backscattering, whereas the transmitted radiation is primarily sensitive to aerosol. Therefore, using combined up- and down-looking observations allows one to simultaneously retrieve the properties of both aerosol and surface with minimal assumptions. In this paper we describe the effort to develop an algorithm for such retrievals, with the objective of deriving new information from ground-based and satellite aerosol observations. Observations of the direct and diffuse transmitted radiation are routinely performed at more than 180 worldwide locations by the AERosol Robotic NETwork (AERONET) of ground-based sun- and sky-scanning radiometers (Holben et al., 1998). The wide spectral and angular range of measurements allows the AERONET inversion algorithm to retrieve an extended set of aerosol parameters, such as particle size distribution, complex refractive index, and single scattering albedo, while making fewer assumptions about aerosol properties than are used in satellite remote sensing (Dubovik & King, 2000). Based on this retrieval approach and the long record of AERONET aerosol measurements, a climatology of

the physical and optical properties of key aerosol types has been developed (Dubovik et al., 2002). However, the AERONET aerosol retrieval relies on an assumed surface reflectivity which is one of the factors contributing to the uncertainty of the derived aerosol properties (Dubovik et al., 2000). Therefore, developing an algorithm that inverts a combination of AERONET observations with coincident satellite measurements could improve the accuracy of aerosol retrieval and, at the same time, provide information about surface reflectance at AERONET sites.

This paper presents an algorithm that retrieves surface reflectance properties (bidirectional reflectance factor, and surface albedo) in addition to aerosol parameters (size distribution, complex refractive index, and single scattering albedo) from AERONET data combined with available satellite observations. For this study we utilized observations from POLDER-2 (ADEOS-2 satellite), MISR, and MODIS (Terra satellite) since these sensors were specifically designed for aerosol and surface characterization. Such an approach aims to maximize the potential fusion of AERONET and satellite observations to compare with common approaches relying on the products of AERONET retrievals alone (Sinyuk et al., 2003).

The paper is organized as follows: Section 2 describes the retrieval algorithm and the technical characteristics of the measurements used for the joint inversion. In Section 3 we present example retrieval results and discuss algorithm robustness by analyzing time series of surface albedo retrieved under different atmospheric conditions. The sensitivity of surface retrievals to the assumptions on aerosol vertical distribution and aerosol particles shape is also discussed. Section 4 analyzes the sensitivity of ground-based aerosol retrievals to the assumptions on surface reflectance. The final section presents a summary and conclusions.

2. Retrieval method

2.1. Measurements

The algorithm retrieves aerosol and surface information from a combination of spatially and temporally collocated AERONET and satellite observations. The number and the values of the wavelengths as well as viewing geometry employed for inversion may vary depending on the satellite observations selected. Therefore, we present a brief discussion of the AERONET and satellite data used in this study. Table 1 summarizes the technical characteristics of each type of measurement.

AERONET radiometers measure aerosol optical depth (from direct sun measurements) and sky radiances using two different observation sequences for acquiring sky radiances: almucantar and principal plane scans (Holben et al., 1998). Almucantar measurements are taken at the elevation angle of the Sun whereas principal plane observations are performed in the Sun azimuthal plane. Optical depth combined with almucantar measurements in four standard AERONET spectral bands (see Table 1) is considered as the basic set of ground-based observations. However, for high Sun elevations, principal plane observations are used instead of almucantar due to the limited range of scattering angles for almucantar measurements, which, according to Dubovik et al. (2000), reduces the aerosol retrieval accuracy. The accuracy of the AERONET aerosol optical depth measurements is ~ 0.01 for the wavelength ≥ 0.44 μm (Eck et al., 1999) and the uncertainty in measured sky radiances due to calibration error is ~5% (Holben et al., 1998).

Observations from three different satellites are selected for combining with AERONET measurements: POLDER-2, MISR, and MODIS. POLDER-2 aboard the ADEOS-2 satellite is a wide field-of-view sensor that takes measurements of top-of-the atmosphere radiance in six spectral channels and degree of linear polarization in three spectral channels (Deschamps et al., 1994). Due to the wide field-of-view POLDER observes any surface point from about 14 different view directions as the satellite passes over a target. Furthermore, after a few days, the successive orbits provide a complete picture of the target BRF (Deschamps et al., 1994). In this study, we use POLDER radiance measurements in only the three spectral channels specifically designed for aerosol characterization (see Table 1). POLDER radiometric calibration accuracy is between 2% up to 4% from the blue to near-infrared channels (Goloub et al., 1999).

The MISR instrument aboard the Terra spacecraft has both multi-wavelength and multi-angle measurement capabilities (Diner et al., 1998). It is equipped with nine cameras pointing in different directions, which observe the reflected radiation field at nine different view zenith angles, each camera making measurements in four spectral bands (see Table 1). In this study we use only the three spectral channels which closely match those of AERONET observations. The absolute radiometric calibration for MISR is <4% according to Bruegge et al. (2006-this issue).

MODIS, also aboard the Terra satellite, performs single view angle observations in a wide spectral range providing images in 36 spectral channels (King et al., 1992). Furthermore, during a

Table 1
Data sets used for joint inversion

Data set	Type of measurements	Number of spectral bands	Wavelengths used in this study, μm	Number of view angles	Range of scattering angles
AERONET	Optical depth	4	0.44, 0.67, 0.87, 1.02	1	N/A
	Sky radiance, almucantar	4	0.44, 0.67, 0.87, 1.02	27	Depends on solar Zenith angle. Maximum range: ~3°–150°
	Sky radiance, principal plane	4	0.44, 0.67, 0.87, 1.02	33	Maximum range: ~3°–140°
POLDER	TOA radiance	3	0.44, 0.67, 0.87,	14	~70°–170°
MISR	TOA radiance	3	0.45, 0.67, 0.87	9	~60°–160° (for mid-latitudes)
MODIS	TOA radiance	4	0.443, 0.67, 0,87, 1.02	1	~70°–170° (1 angle each day)

16-day period MODIS is capable of building up several sequential angular views of a given surface target (Schaaf et al., 2002). In this study, we use the MODIS measurements in four spectral bands that are the closest to those of AERONET sunphotometers (see Table 1). The uncertainties in the MODIS measured reflectance in the visible and mid-infrared channels are less than 2% (Guenther et al., 2002).

Due to the their multi-directionality, measurements from MISR and POLDER sensors are expected to supplement AERONET observations better than one-directional MODIS observations, and therefore are considered as the basic data sets for joint inversion. However, in situations when MISR and POLDER coincident data are not available then the MODIS observations are used.

Both ground-based and satellite observations are cloud screened before inferring aerosol and surface information. The cloud-free data are identified by cloud screening algorithms of both AERONET (Smirnov et al., 2000) and the corresponding satellite instruments.

Satellite and ground-based observations are collocated in space by selecting the satellite pixel nearest to the AERONET site location. Then the ground-based measurements closest in time to the satellite overpass, and separated by no more than 30 min, were used for joint processing.

2.2. Retrieved parameters

The aerosol information retrieved is similar to that derived by the standard AERONET retrieval algorithm (Dubovik & King, 2000; Dubovik et al., 2000). It includes the aerosol volume size distribution in the total atmospheric column, and aerosol complex refractive index at both AERONET and satellite spectral channels. Using this microphysical information, single scattering albedo is calculated as a function of wavelength. The retrieval method assumes no restrictions on the number of modes or the type (e.g. log-normal, etc.) of the aerosol size distribution, which is parameterized by values in 22 independent size bins in the range: $0.05 \le r \le 15$ μm, where r represents particle radius. Also, no predetermined spectral dependence is assumed in the retrieved aerosol complex refractive index. Only spectral and size smoothness constraints are used, preventing unrealistic oscillations in either parameter (Dubovik & King, 2000). The aerosol is modeled as a mixture of homogeneous spherical particles with the exception of desert dust cases where accounting for particle non-sphericity is necessary. The desert dust aerosol is modeled as a mixture of randomly oriented polydisperse spheroids (Mishchenko et al., 1997) with shape (aspect ratio) distribution fixed, based on a desert dust polarimetric measurements analysis (see details in the paper by Dubovik et al. (2006)). Detailed discussion of the assumptions used in aerosol model parameterization (for example, assigning the same complex refractive index to all size bins) and their impact on retrieval results can be found in (Dubovik et al., 2000).

In addition to aerosol properties, the method also retrieves spectral bidirectional reflectance factors (BRF) and surface albedo. For inversion purposes it is important to describe bidirectional surface reflectance in terms of a limited number of parameters, which can be done with a number of analytical models reported in the literature (e. g. Lucht & Roujean, 2000; Roberts, 2001). For this study the Rahman–Pinty–Verstraete (RPV) model (Rahman et al., 1993) was employed. This model performs well over a variety of land surface covers (e. g. Maignan et al., 2004; Privette et al., 1997; Rahman et al., 1993). This is a three-parameter semi-empirical model, based on the product of three functions: (i) a modified Minnaert function (Minnaert, 1941) which is a combination of the view and illumination zenith angles, (ii) a one-term Henyey and Greenstein function (Henyey & Greenstein, 1941) accounting for the phase function of the scattering elements, and (iii) a hot spot function describing the increase of surface reflectance in the direction of the illumination:

$$\rho_S(\vartheta_1,\varphi_1;\vartheta_2,\varphi_2) = \rho_0 \frac{\cos^{k-1}\vartheta_1 \cos^{k-1}\vartheta_2}{(\cos\vartheta_1+\cos\vartheta_2)^{1-k}} F(g)[1+R(G)] \tag{1}$$

$$F(g) = \frac{1-\Theta^2}{[1+\Theta^2-2\Theta\cos(\pi-g)]^{1.5}} \tag{1a}$$

$$\cos g = \cos\vartheta_1\cos\vartheta_2 + \sin\vartheta_1\sin\vartheta_2\cos(\varphi_1-\varphi_2) \tag{1b}$$

$$1+R(G) = 1+\frac{1-\rho_0}{1+G} \tag{1c}$$

$$G = [\tan^2\vartheta_1 + \tan^2\vartheta_2 - 2\tan\vartheta_1\tan\vartheta_2\cos(\varphi_1-\varphi_2)]^{1/2} \tag{1d}$$

where ϑ_1, φ_1 and ϑ_2, φ_2 represent zenith and azimuth angles for illumination and observation directions respectively, g is the phase angle. Eqs. (1), (1a), (1b), (1c), and (1d) constitute the RPV model which describes the surface bidirectional reflectance in terms of three independent parameters: ρ_0, k, and Θ. The parameters ρ_0 and k represent the intensity of the surface reflectance and the level of surface reflectance anisotropy, respectively. The coefficient Θ determines the relative amount of forward and backward scattering. In our approach the parameters ρ_0, k, and Θ are retrieved for the satellite spectral channels. The following ranges of variability of these parameters were assumed based on results of fitting of field observations by the RPV model (e. g. Rahman et al., 1993):

$$0.001 \le \rho_0 \le 0.99 \tag{2a}$$

$$0.1 \le k \le 1 \tag{2b}$$

$$-0.5 \le \Theta \le 0.5 \tag{2c}$$

No specific restrictions on spectral dependence of these parameters are assumed other than spectral smoothness constraints. The RPV parameters are retrieved from combinations of AERONET measurements with MISR and/or POLDER multi-directional observations. Then the BRF and surface albedo are calculated. For a joint AERONET/MODIS inversion, the

Lambertian approximation is used since MODIS lacks same day multi-angle capability to retrieve BRF from one day only.

2.3. Retrieval algorithm

The inversion implementation is similar to that used in the standard AERONET retrieval algorithm. Therefore, we present just a brief description of the basic principles of the approach. Additional details can be found in Dubovik and King (2000), Dubovik et al. (2000), and Dubovik (2004).

According to the general inversion strategy adopted in Dubovik and King (2000), the results are derived from a complex data set that includes both the AERONET and satellite measurements and *a priori* data constraining the retrieval results. The inversion algorithm is designed as multi-term Least Squares Method (Dubovik, 2004) that searches for the best fit of the theoretical model to several measurement and a priori data sets. It is statistically optimized to minimize the effect of random errors, and takes into account the different levels of accuracy of the data from different sources. The method assumes a log-normal error distribution for all input data, i.e., all measurements and retrieved parameters are analyzed in logarithmic space. The best solution corresponds to a minimum of the following quadratic form (Dubovik, 2004; Dubovik & King, 2000; Dubovik et al., 2000):

$$\Psi(\mathbf{a}) = \frac{1}{2}\sum_{k=1}^{9} \gamma_k \left\{ [\mathbf{f}_k^* - \mathbf{f}_k(\mathbf{a})]^T (\mathbf{W}_k)^{-1} [\mathbf{f}_k^* - \mathbf{f}_k(\mathbf{a})] \right\}, \quad (3)$$

where the vector **a** contains the retrieved parameters: the logarithms of the retrieved values of the size distribution function in nodal points, the logarithms of the real and imaginary parts of the aerosol refractive index at the wavelengths selected, and the logarithms of the RPV model parameters at the wavelengths selected. According to Eq (2c) RPV parameter Θ can take negative values. Therefore for working in logarithmic space a simple transformation $(1+\Theta)$ was used. The vectors $\mathbf{f}_k^*$ and $\mathbf{f}_k(\mathbf{a})$ represent measurements of k-th type and fitting respectively. The vector $\mathbf{f}_1$ corresponds to the logarithms of optical depth $\tau(\lambda)$ at the selected wavelengths, the vectors $\mathbf{f}_2$ and $\mathbf{f}_3$ correspond to the logarithms of the AERONET $I_{\mathrm{AER}}(\lambda,\vartheta)$ and satellite $I_{\mathrm{SAT}}(\lambda,\vartheta)$ radiance measurements at the selected wavelengths and angles, respectively, the vector $\mathbf{f}_4$ includes the size distribution smoothing function values at the nodal points, the vectors $\mathbf{f}_5$ and $\mathbf{f}_6$ contain the aerosol complex refractive index (real and imaginary part) smoothing functions, respectively, and $\mathbf{f}_7$, $\mathbf{f}_8$, and $\mathbf{f}_9$ are the smoothing functions for the RPV model parameters. The matrices $\mathbf{W}_k$ are the weighing matrices of random errors in the individual data sets. The Lagrange multipliers γ_k are defined from statistical considerations and represent the relative contributions of the k-th type measurements to the joint data set

$$\gamma_k = \frac{\varepsilon_2^2}{\varepsilon_k^2}, \quad (4)$$

where ε_k^2 denotes the variance of errors for the data vector $\mathbf{f}_k^*$. In the retrieval algorithm the quadratic form (3) is normalized to the error of AERONET sky measurements ε_2^2, using the following expression (Dubovik & King, 2000)

$$\frac{2\Psi(\mathbf{a})}{(N_f - N_a)} = \varepsilon_2^2, \quad (5)$$

where N_f is the number of values in all vectors $\mathbf{f}_k^*$, and N_a is the number of retrieved parameters.

To derive aerosol and surface information from the combined data set, the radiative characteristics of the atmosphere are modeled in the retrieval algorithm (Dubovik et al., 2000). The modeling was done using a version of the Discrete–Ordinate radiative transfer code by (Nakajima & Tanaka, 1986, 1988) that accurately accounts for bi-directional surface reflectance, molecular and aerosol multiple scattering. Weak gas absorption (ozone) is accounted for from climatological data (Holben et al., 1998). Accounting for the vertical variability of aerosol properties is important for correctly modeling atmospheric radiation. The standard AERONET retrieval algorithm adopts a simple model of a homogeneous atmosphere that assumes constant aerosol properties within the entire atmospheric column. It constitutes a reasonable assumption for almucantar measurements, since all atmospheric layers are always viewed with similar geometry. In contrast, both AERONET measurements in the principal plane and satellite observations are sensitive to aerosol vertical distribution at short wavelengths (e. g. Gordon, 1997; Holben et al., 1998; Quijano et al., 2000). In this study a range of aerosol vertical distributions was assumed. The particular aerosol vertical profiles selected for our retrievals are described in Section 3.1.

3. Results

We applied this retrieval method to joint sets of ground-based and satellite observations over two AERONET sites: Mongu, Zambia during August 2003 and Solar Village, Saudi Arabia during June 2003. These sites represent different aerosol types. Over Mongu the atmospheric loading is dominated by biomass burning aerosols, whereas at the Solar Village, it is dominated by desert dust. Due to the relatively small solar zenith angles corresponding to the time of satellite overpass for the selected sites (~40° for Mongu and ~16° for Solar Village), the AERONET principal plane measurements were used for the ground-based observations.

3.1. Aerosol vertical distribution

Before processing the data, we refined our assumptions about aerosol vertical distribution. As a starting point, micro-pulse lidar network (MPLNET) observations performed during SAFARI 2000 field campaign at Mongu were used (e. g. Campbell et al., 2003; McGill et al., 2003). These observations over the Mongu are available at the MPLNET website (http://mplnet.gsfc.nasa.gov) and exhibit a variety of shapes, and highly temporally variable aerosol vertical distributions. Based on a large number of cases, we used the following general features to model the aerosol vertical distribution: 1) aerosol is mostly

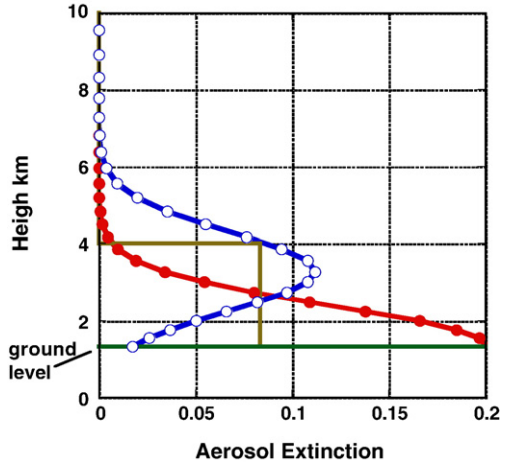

Fig. 1. Normalized extinction profiles used to model aerosol vertical distribution. Solid line and lines with solid and open circles depict homogeneous aerosol distribution and Gaussian aerosol profiles with maximum at ground level and at 3 km respectively.

concentrated within 4 km of sea level, and 2) the range of vertical profiles could be separated into roughly three different groups. The first group includes aerosol vertical distributions having maximum aerosol concentration close to ground level, and, represents local fires. The second and third groups combine elevated layers and well-mixed aerosol, respectively, and could be typical of transported smoke. Based on this information, we selected three different aerosol vertical distributions, presented in Fig. 1: a homogeneous distribution with 4 km width, and two Gaussian profiles with 1 km width and maximum aerosol concentrations at ground level and at 3 km respectively. Performing retrievals for each selected profile allows us to analyze the influence of the aerosol vertical distribution on the retrieval results.

In modeling aerosol vertical distribution only the variability of aerosol concentration is assumed. Other aerosol properties (particle size distribution, complex refractive index) are considered to be constant. Since assumed profiles are representative of rather general scenarios of the aerosol vertical distribution, they are also used to model vertical variability of aerosol at Solar Village, where lidar data are not available.

3.2. Fitting of the measurements

As mentioned in Section 2, our retrieval approach is based on the simultaneously fitting a joint set of observations with a theoretical model. Therefore, the quality of fit is the most important criterion for identifying successful retrievals. Retrievals are considered successful only if residual values calculated by Eq. (5), are no greater than 3–5%, the expected measurements accuracy. Figs. 2 and 3 present examples of fitting of the AERONET and satellite observations at the Mongu site.

3.3. Examples of surface retrievals

This section focuses on surface BRF and albedo retrievals as new retrieval products compared to aerosol parameters routinely provided by AERONET. In the analysis of retrieved surface properties, we compare retrievals from joint observations of AERONET and different satellites to the MISR surface reflectance product for the same or similar observation times. This strategy tests the consistency of different retrievals.

Fig. 4 presents BRF (left panel) and surface albedo (right panel) retrieved at the Mongu site, assuming a homogeneous vertical aerosol distribution (see Fig. 1). In this example and throughout the paper the term surface albedo stands for directional hemispherical reflectance (DHR). This quantity is calculated after removing atmospheric scattering effects and constitutes an intrinsic surface property (e. g. Pinty et al., 2005). Before inverting the data, MISR and MODIS spatial resolutions were aggregated to 6 km by 6 km, to match the spatial resolution of POLDER at nadir. In the left panel, the BRFs retrieved from the joint observations of AERONET with POLDER and MISR are compared to the MISR operational retrieval. The results are presented in the plane defined by the MISR viewing directions, which is close to the solar principal

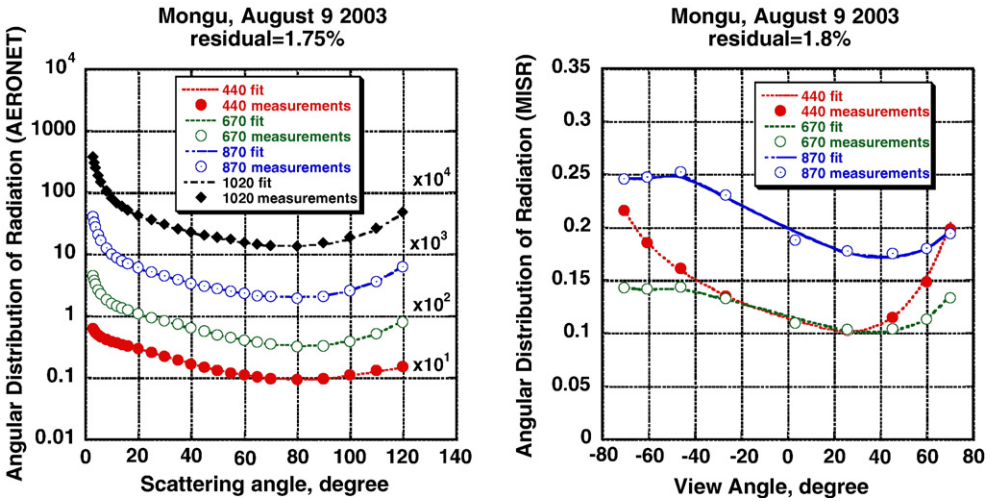

Fig. 2. An example showing simultaneous fits to the AERONET (left) and MISR (right) observations.

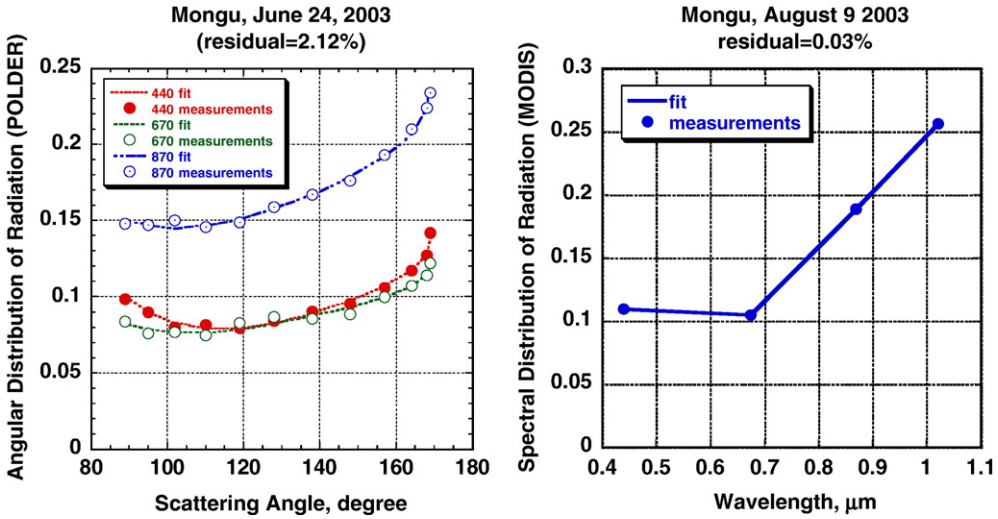

Fig. 3. An example showing fits to the POLDER (left) and MODIS (right) observations.

plane (Fig. 5). Fig. 4a shows that for all the spectral channels, the retrievals produce consistent BRF angular shapes, including a hot-spot maximum near 40° view angle (the solar zenith angle ~40°). The agreement in reflectance magnitude changes with spectral channel and observation set. The MISR and AERONET/MISR retrievals agree closely with each other at all of the wavelengths, as do the POLDER and AERONET/POLDER retrievals. However, the MISR- and POLDER-based retrieval pairs do not agree as well at longer wavelengths. This discrepancy must be due to differences in the MISR and POLDER signals because observations from the same sensors provide consistent results. Among the possible factors responsible for the MISR–POLDER observation discrepancies are differences in angular sampling (Fig. 5), satellite pixel geo-location, spatial resolution, and radiometric calibration. The difference in angular sampling could possibly explain some of the discrepancies in magnitude of reflectance at BRF maximum, because the POLDER observation plane is farther from the solar principal plane and the hot-spot position as illustrated by Fig. 5. It would require a rather large difference in radiometric calibration to generate a disagreement of this magnitude. Some of the differences between MISR and POLDER-based BRF retrievals could be explained by a difference in satellite pixels geo-location and spatial resolution; these are especially important due to surface heterogeneity at the Mongu site (Fig. 6). These factors, however, are less important for the consistency of POLDER-based retrievals because POLDER-2 observes the same part of the Earth surface every four days.

The right panel of Fig. 4 shows the surface albedos corresponding to the retrieved BRFs. It also presents surface albedo retrieved from the combination of AERONET and MODIS data by using the Lambertian approximation. As with the BRFs, the surface albedo retrievals derived from different observations agree at short wavelengths. At the longer wavelengths, the

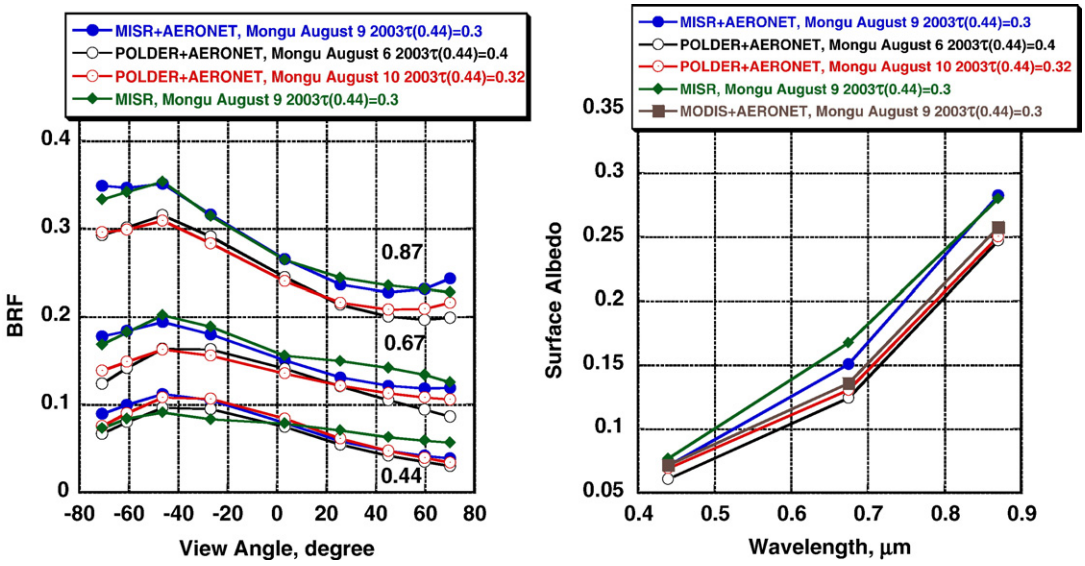

Fig. 4. BRF and surface albedo retrievals at the Mongu site. A homogeneous aerosol vertical distribution was assumed.

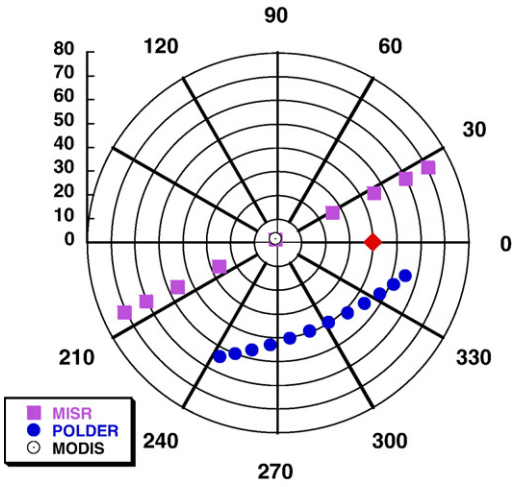

Fig. 5. Angular sampling of the MISR, POLDER, and MODIS observations used for the joint inversion at the Mongu site. The radius represents viewing zenith angle in degrees, and the polar angle, the relative azimuth between the Sun and view directions. The diamond represents the average Sun position for the data sets so the solar principal plane is along 0°–180° axis.

MISR and AERONET/MISR retrievals are higher than those from the AERONET/POLDER combination, which reflects the behavior of the corresponding BRF.

Examples of Solar Village surface retrievals are shown in Fig. 7, BRF in the left panel, and surface albedo on the right panel. BRF retrievals are also presented in the plane generated by the MISR viewing directions. In a contrast to Mongu case, this plane is almost perpendicular to the solar principal plane, as illustrated by Fig. 11. This presents the most unfavorable conditions for BRF retrievals, especially angular shape, because the main variability of surface reflectance is concentrated in solar principal plane. In this case, additional assumptions could be required to constrain the solution. Indeed, our first retrieval attempts produced BRFs having angular shapes at short wavelengths that were significantly different from the BRF angular shapes at longer wavelengths. In general, some wavelength dependence of surface reflectance angular anisotropy is expected due to the spectral dependence of absorption and transmittance of radiation by scattering elements (soil grains, green leaves etc), which becomes important in the presence of multiple scattering (e. g. Lyapustin et al., 2006). For example, this is the case for vegetated surfaces, where transmittance and absorption of radiation by green leaves are different in visible and near-infrared parts of solar spectrum (e. g. Deering et al., 1999). The contribution of multiple scattering within three-dimensional vegetation structure is significant due, in particular, to the non-zero transmittance of light by leaves. In the case of soil surfaces, the absorption of radiation is stronger in the blue part of spectrum, but there is little transmittance in all wavelengths. It reduces the amount of multiple scattered radiation, and consequently its effect on spectral variability of bi-directional surface reflectance. This consideration is supported by the results of Irons et al. (1992) where the spectral similarity in angular shape of soil bi-directional reflectance factor was experimentally observed. Therefore, we adopted some constraints on the spectral dependence of the BRF shape. This strategy was suggested by Diner et al. (2005), who found that forcing spectral invariance of the BRF angular shape improves MISR aerosol and surface retrievals. Hence, in retrieving surface reflectance at Solar Village we restricted the spectral variability of the BRF angular shape a priori. Specifically, we applied limitations on the derivatives of the spectral dependence of the k and Θ parameters that determine the angular shape of BRF in the RPV model. The strength of spectral smoothness constraints is driven by the values of the corresponding Lagrange multipliers (Eq. (4)) which could be adjusted once more detailed *a priori* information on spectral variability of bi-directional surface reflectance became available. These constraints are technically similar to those used by Dubovik and King (2000) for constraining the spectral variability of the complex refractive index of aerosol particles. The methodology of using such constraints is described in details by Dubovik (2004).

The left panel of Fig. 7 shows that BRF retrievals in the 0.44 μm spectral channel are consistent both in terms of reflectance magnitude and shape. At longer wavelengths, the retrievals also agree well, especially at the BRF maximum. Some discrepancy at the BRF wings could be partly explained by differences in aerosol characterization. In the case of the joint inversion, aerosol properties are strongly constrained by ground-based measurements, whereas satellite-based retrievals rely on a set of pre-selected aerosol models. The right panel of Fig. 7 illustrates qualitatively good agreement among the surface albedo retrievals.

Fig. 6. Photograph taken at the AERONET site at Mongu, Zambia.

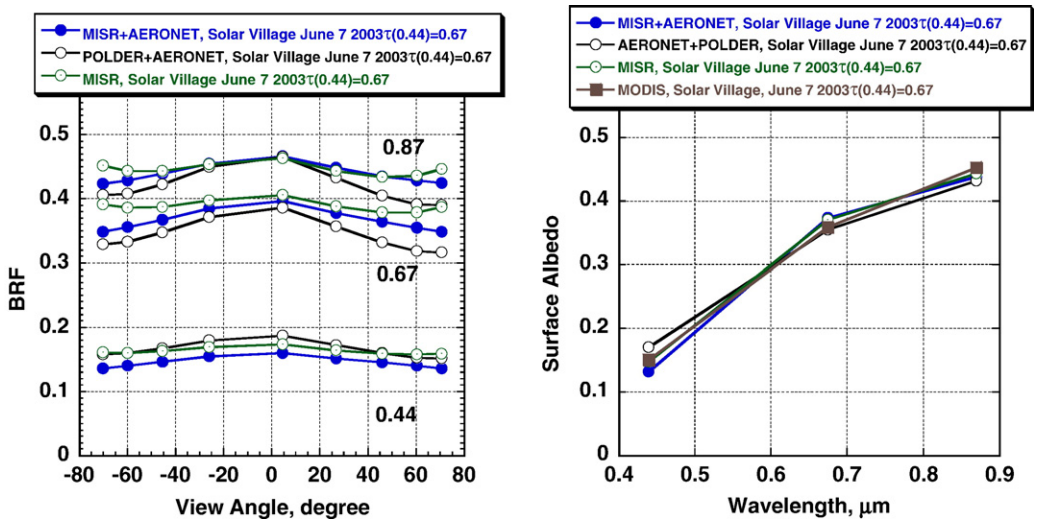

Fig. 7. BRF and surface albedo retrievals at the Solar Village site. A homogeneous aerosol vertical distribution was assumed.

3.4. Testing algorithm robustness

Aerosol loading, important in itself, is also a key factor affecting the accuracy of surface reflectance retrievals. Indeed, the sensitivity of top-of-atmosphere reflectance observations to surface properties is reduced when aerosol optical depth is high because the satellite signal is dominated by the aerosol contribution. Therefore, one can expect that the strong aerosol optical depth variability could affect the stability of BRF retrievals, for example, by inducing temporal variability in surface retrievals correlated with significant aerosol loading variations. In this section we examine algorithm performance under variable aerosol loading conditions.

We analyzed the time series of surface albedo retrievals obtained for a time period when no significant variability of surface reflectance is expected. In addition, high aerosol optical depth temporal variability during the selected period provides conditions favorable for testing algorithm robustness. Low seasonal variability of surface properties is usually expected for desert surfaces at the Solar Village AERONET site and at the forest savanna Mongu site in the middle of the dry season in August (e. g. Holben et al., 2001). The low-temporal-variability-of-surface-reflectance assumption during certain time periods is commonly employed by surface characterization algorithms (e. g. Lyapustin et al., 2006). For instance, MODIS uses a 16-day period to accumulate observations for BRF retrievals (Schaaf et al., 2002).

Fig. 8 shows the temporal dependence of surface albedo retrieved at the Mongu, using the three aerosol vertical distributions described in Section 3.1. AERONET and POLDER observations were selected for the joint inversion because they provide the largest number of collocated measurements. The selected time period is characterized by strong temporal aerosol loading variability; the optical depth at 0.44 μm ranges from about 0.2 to 1. As is seen from Fig. 8, retrievals at longer wavelengths are very stable, showing no dependence on aerosol vertical distribution. In a contrast, at 0.44 μm the retrieved surface albedo depends on the aerosol profile assumption and also exhibits peaks correlated with variations in aerosol optical depth. Such dependence of satellite observations, and consequently surface retrievals, on aerosol vertical distribution can be explained by contributions from multiple scattering interactions between aerosol and vertically stable Rayleigh (molecular) scattering (e. g. Gordon, 1997; Torres et al., 2005). The strength of these interactions at a particular wavelength depends on the magnitude of both the Rayleigh and aerosol optical depth. The Rayleigh optical depth is high in near UV, and rapidly decreases with wavelength, which explains the different surface retrievals sensitivity to aerosol vertical distribution in the short and long spectral channels. In spectral regions having strong Rayleigh scattering, the sensitivity to aerosol vertical structure increases

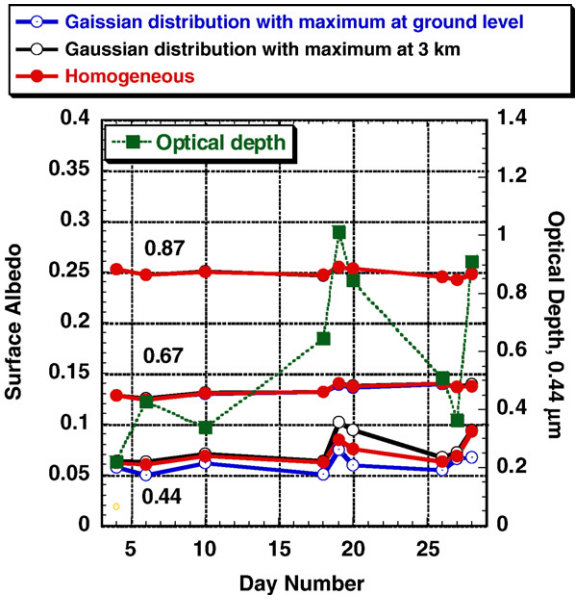

Fig. 8. Surface albedo time series, retrieved from joint AERONET and POLDER observations, for Mongu during August 2003.

with aerosol optical depth as illustrated in Fig. 8. The effect of aerosol vertical distribution on surface retrievals is discussed in the next section.

To better understand the nature of the peaks in surface albedo temporal dependence at 0.44 μm the retrievals were plotted as a function of aerosol optical depth in Fig. 9 and the surface albedo retrievals were separated into two groups by aerosol optical depth. The first group corresponds to optical depth values less than 0.5 and the retrieved surface albedo does not exhibit significant correlation with optical depth: $R^2=0.15$, 0.003, and 0.009 for the homogeneous aerosol distribution and Gaussian aerosol profiles with the maxima at the ground level and at 3 km respectively. The second group combines surface albedos retrieved at optical depth larger than 0.5, and demonstrates very strong correlation: $R^2=0.97$, 0.93, and 0.72. This simple analysis shows that at small and moderate aerosol optical depth the surface retrievals are not significantly affected by aerosol loading, which however becomes important for aerosol optical depth above a certain threshold. In the Mongu case, this threshold value is estimated to be between 0.65 and 0.85 at 0.44 μm, as illustrated by Fig. 9. For longer wavelengths, the maximum aerosol optical depth is below the estimated limit (0.54 and 0.30 at 0.67, and 0.87 μm respectively) which explains the stability of the corresponding surface albedo retrievals.

As discussed before, decreased satellite measurement sensitivity to surface properties is a possible reason for the correlation between surface albedo retrieval and aerosol optical depth. To evaluate that effect, we performed a number of numerical tests. Ground-based and satellite observations were simulated for aerosol optical depth at 0.44 μm varying from 0.7 to 2.5. These synthetic observations then were used as an input to the inversion code, and errors in retrieved surface albedo were analyzed. The analysis showed a significant loss of sensitivity for values of aerosol optical depth larger than 1.5, resulting in albedo retrieval errors greater than 0.02. Since the observed optical depth values at Mongu are lower than 1.5 we

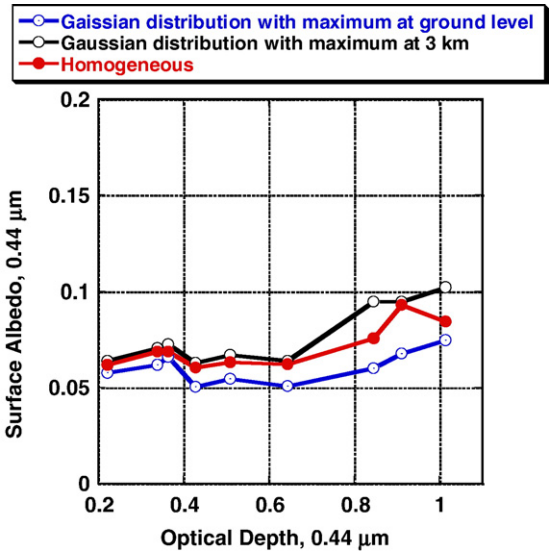

Fig. 9. Dependence of retrieved shortwave surface albedo on aerosol optical depth, at the Mongu site.

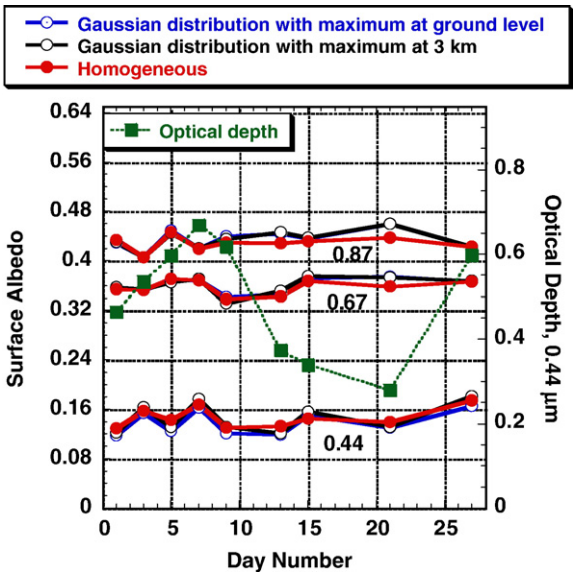

Fig. 10. The same as Fig. 8, but for Solar Village site.

conclude that the correlation of retrieved surface albedo with optical depth cannot be explained by low satellite sensitivity to surface reflectance. Instead, we considered the following factors which could potentially contribute to the positive correlation of retrieved surface albedo with aerosol optical depth: satellite calibration errors, uncertainty in aerosol vertical distribution and shadowing effect (Deering & Eck, 1987). The influence of the first two factors on surface albedo retrievals was evaluated by numerical tests using the following strategy. Ground-based and satellite observations were simulated with a homogeneous aerosol profile (Fig. 1) for two (minimal and maximal) values of aerosol optical depth observed at Mongu site. Then constant biases representing calibration errors have been added to simulated satellite observations: ±4, 2, and 2% for 0.44, 0.63, and 0.67 μm respectively (based on estimates from the POLDER science team). These synthetic data were used as an input for inversion, and the results were analyzed by comparing the difference between the values of surface albedo retrieved under two aerosol loadings to the corresponding difference observed in the joint retrievals. The effect of uncertainty in aerosol vertical distribution on surface albedo retrievals was estimated by inverting synthetic observations with two Gaussian profiles depicted in Fig. 1. The results of numerical tests showed that positive correlation between the values of retrieved surface albedo and aerosol optical depth could be achieved only if the bias in satellite calibration is positive. Negative bias in satellite calibration resulted in negative correlation of surface albedo retrievals with aerosol loading regardless of assumed aerosol profile. In the case of positive calibration bias, the uncertainty in aerosol vertical distribution explained ~97% of surface albedo retrievals variability with aerosol loading observed in the joint retrievals. The absolute error in retrieved surface albedo at 0.44 μm varied with aerosol profile from ~0.012 to 0.018 (low aerosol loading) and from ~0.021 to 0.04 (high aerosol loading). The results of numerical tests for longer wavelength channels showed lower sensitivity of the surface albedo retrievals to the combined uncertainty in satellite

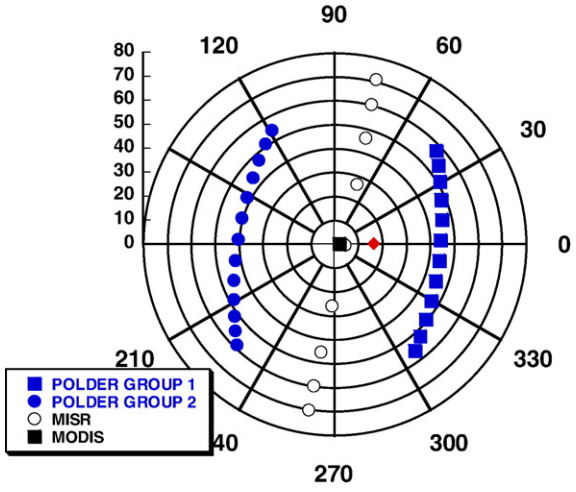

Fig. 11. The same as Fig. 5, but for Solar Village site.

calibration and aerosol vertical distribution with typical errors less than 0.01.

Though the remaining 3% in observed variability of retrieved surface albedo with aerosol optical depth is at the level of measurements accuracy we found it useful to mention one more factor which could potentially contribute to the increase of retrieved values of surface albedo with aerosol optical depth: the shadowing effect, observed experimentally by Deering and Eck (1987). According to Deering and Eck (1987), the effect is important for surfaces having fractional leaf canopy coverage, which is the case for Mongu (Fig. 6). For this type of surface, the shadowing of background (soil, dead brown vegetation) by the canopy decreases with increased aerosol optical depth, due to the accompanying increase in diffuse sky irradiance, allowing more radiation to be reflected by the background. Since the background reflection in the visible is much higher than the reflection by green leaves, the surface total scene reflectance will be higher on the hazy days, as less background is covered in shadows. Evaluation of the shadowing effect contribution is difficult without estimation of its magnitude, which involves theoretical modeling of atmospheric radiation interaction with heterogeneous surface and is beyond the scope of this paper.

The temporal dependence of surface albedo retrieved at Solar Village from the combination of AERONET and POLDER observations is presented in Fig. 10. The surface albedo retrievals in all spectral channels show temporal variability that is not correlated with variations in aerosol optical depth. This could be explained by the difference in POLDER angular sampling for different days. Fig. 11 shows that in terms of angular sampling, all the POLDER observations used in the joint inversion can be separated into two different groups having different sets of relative azimuth angles: from ~50° to ~300° (group 1) and from ~120° to ~230° (group 2). Plotting the retrieval results separately for each group significantly reduces the temporal variability of surface albedo, as illustrated in Fig. 12.

Fig. 10 also shows that, in contrast to the Mongu case, the surface albedo retrieved at 0.44 μm does not exhibit substantial dependence on the assumed aerosol vertical distribution. This could be explained by the difference in shortwave surface albedo for these two sites: 0.06 and 0.14 in average for Mongu and Solar Village, respectively. In the later case variations in satellite signal due to changes in aerosol vertical distribution are less important over a brighter surface reflectance background. Additionally, aerosol optical depths are not as high for the Solar Village case and the influence of the assumed vertical aerosol profile increases as aerosol optical depth increases.

A numerical test for Solar Village was performed to study whether the effect of the combined uncertainty in satellite calibration and aerosol vertical distribution on the surface albedo retrievals is consistent with the results of the joint inversion. The absolute error in 0.44 μm surface albedo retrievals varies with aerosol profile from ~0.012 to ~0.014 and from ~0.014 to ~0.024 for low and high aerosol optical depth respectively.

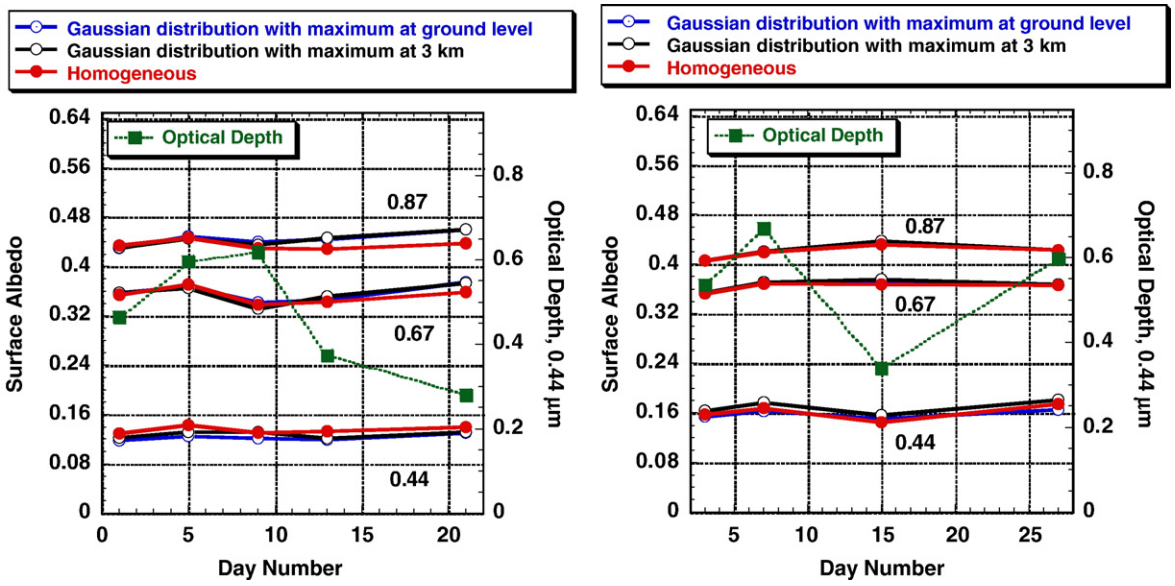

Fig. 12. The same as Fig. 10, but for two groups of POLDER angular samples. The right panel shows retrieval results for group 1, the left for group 2.

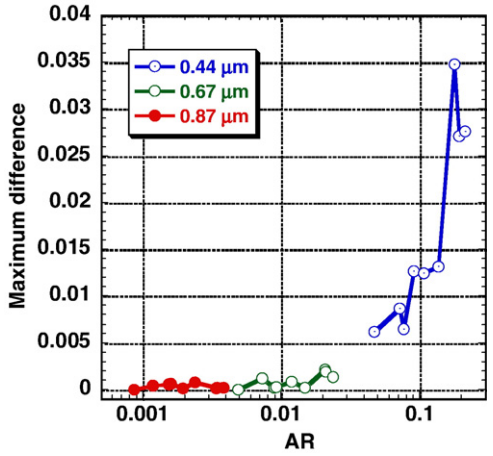

Fig. 13. Dependence on the AR parameter of the maximum retrieved surface albedo difference produced by assumed aerosol vertical distribution. The AR parameter is defined as the product of the aerosol and Rayleigh optical depths.

This results in relative variability of the retrieved surface albedo with aerosol loading on the order of 0.01 or less. For longer wavelengths the typical error in surface albedo retrievals due to this combined uncertainty is less than 0.01.

In conclusion, we would like to briefly discuss one more factor that could affect both aerosol and surface retrievals at 0.44 µm: neglect of polarization in radiative transfer modeling of atmospheric radiation. According to Lacis et al. (1998) and Mishchenko et al. (1994), scalar approximation of radiative transfer (e. g. DISORT used in this study) is known to introduce errors in computed radiances. The error introduced by the use of scalar code can reach 5–10% in both directions (over and under estimation) especially for a clear atmosphere where Rayleigh scattering dominates (Lacis et al., 1998). This effect is more critical in the inversion of observations for low optical depth at 0.44 µm since aerosol and the land surface reflectance effect on upward radiances reduces the overall polarization. The discrepancies observed in simulated radiances can reach 10% in the backscattering, however the average bias observed is reduced due to a change of sign of the error, and typically is of the order of 3%. To address that issue we plan to implement a newly developed vector radiative transfer code (6SV, Kotchenova et al., 2006) for joint inversion processing in the future.

3.5. Surface retrievals sensitivity to the aerosol model assumptions

The theoretical assumptions made in radiative transfer modeling of the Earth–atmosphere system could affect the accuracy of both the aerosol and surface retrievals. Normally, these assumptions are difficult to constrain without employing additional information. In cases when such information is unavailable or incomplete, the usual approach is to analyze the sensitivity of retrieval results to the assumptions by varying the corresponding parameters within physically reasonable ranges. Here surface retrieval sensitivity to assumptions about aerosol vertical distribution and particle shape is analyzed.

The absolute differences in surface albedo values retrieved with different aerosol vertical distribution assumptions were calculated for all the days and wavelengths of the cases shown in Fig. 8. Then, the maximum differences were selected and plotted as a function of the product of the aerosol and Rayleigh optical depths, which we further reference as parameter AR, in Fig. 13. This representation makes it possible to quantify the effect of aerosol vertical distribution on surface albedo retrieval without explicit dependence on wavelengths used for observations and demonstrates an exponential-like increase of the maximum difference with parameter AR. The effect is very small for long wave retrievals due to low values of Rayleigh optical depth. At 0.44 µm there is a sharp increase in the maximum difference with increasing parameter AR, caused by the combined increase in Rayleigh and aerosol optical depth at shorter wavelengths. In this case, for a value of parameter AR as

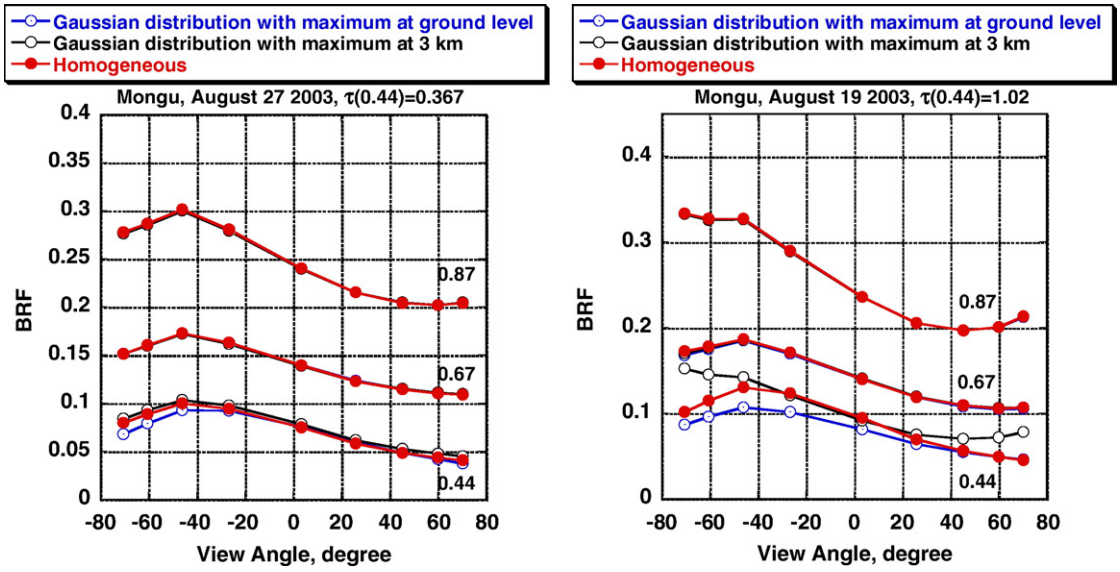

Fig. 14. Illustration of BRF retrieval sensitivity to assumed aerosol vertical distribution.

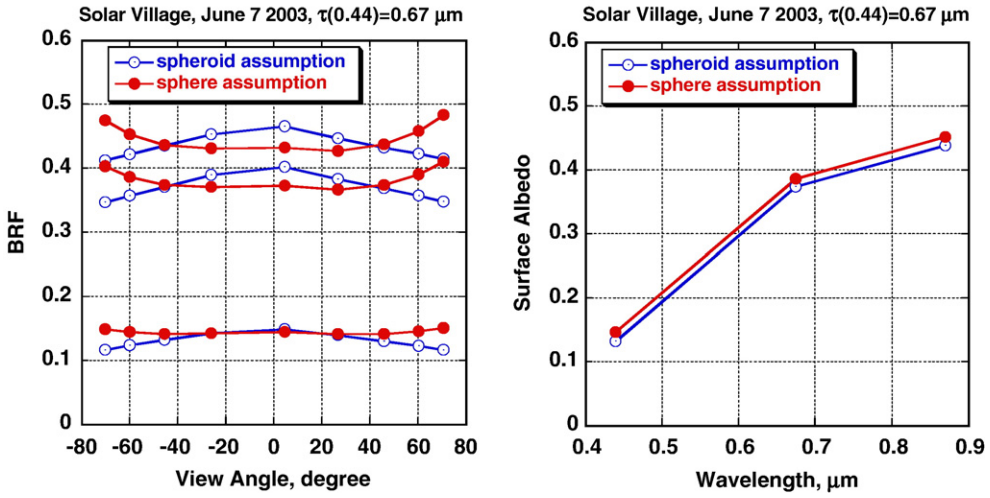

Fig. 15. Illustration of surface retrieval sensitivity to assumed particle shape.

high as ~0.15 (aerosol optical depth at 0.44~0.7 μm), the maximum difference in retrieved surface albedo due to the assumed aerosol vertical distribution does not exceed 0.02, the value often considered as an accepted tolerance error of climatic models (e. g. Sellers, 1993). Further increase in the parameter AR produces larger maximum differences, with a peak value of 0.035 for aerosol optical depth close to 0.85.

The aerosol vertical distribution assumption also affects the retrieved shortwave BRF, as shown in Fig. 14 for two cases having different aerosol loading. Under low aerosol loading, changes in aerosol vertical structure result in only minor variability of both magnitude and angular shape of retrieved shortwave BRF. For higher aerosol optical depth, the aerosol vertical distribution significantly affects both the magnitude and the angular shape of the 0.44 μm BRF, as illustrated by the right panel of Fig. 14.

Numerous studies indicate the necessity of accounting for particle non-sphericity in remote sensing of desert dust (e. g. Dubovik et al., 2003; Herman et al., 2005; Kalashnikova et al., 2005; Kalashnikova & Sokolik, 2002; Mishchenko et al., 2002). The reflection of light by aerosol into the backscattering hemisphere is particularly sensitive to particle non-sphericity. Therefore, retrieving surface properties from satellite data, with algorithms that assume spherical particles can misinterpret the effect of particle non-sphericity as a change in surface reflectance contribution. To account for aerosol particle non-sphericity, we use the randomly oriented spheroids model introduced in (Mishchenko et al., 1997). This simple model reproduces the main light scattering features of natural mineral dust particles by choosing the appropriate spheroid shape distribution (Mishchenko et al., 1997) and was successfully applied in operational AERONET retrievals (Dubovik et al., 2002). In this study we use the refined spheroid mixture derived by Dubovik et al. (2006), from laboratory polarimetric measurements of Volten et al. (2001).

The particle shape sensitivity analysis was performed by inverting joint observations at the Solar Village site. To ensure that aerosol loading is mostly dominated by dust, only observations having Angstrom exponent less than 0.2 were used. Retrievals were made using both spheroid and spherical models, and the surface retrieval differences produced by these particle shape assumptions were analyzed. The left panel of Fig. 15 shows that non-sphericity strongly affects the shape of the retrieved BRF, producing a transition from a bowl-like shape for spheres to a bell-like shape for spheroids. The difference is significant for all spectral channels, and is due to the difference in spherical and non-spherical aerosol phase functions. The right panel of Fig. 15 shows that surface albedo retrievals are almost independent of particle shape assumptions. This is consistent with the BRF shapes, since angular differences at large and small view angles compensate for each other.

4. Sensitivity of AERONET aerosol retrievals to surface reflectance

The sensitivity of AERONET aerosol retrievals to surface reflectance was first analyzed in Dubovik et al. (2000). It was

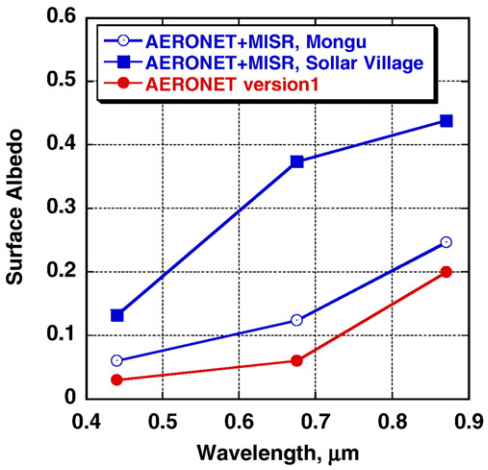

Fig. 16. Comparison between the surface albedo retrieved with the joint inversion, for Mongu and Solar Village, and the surface albedo assumed by version 1 of the AERONET aerosol retrieval algorithm.

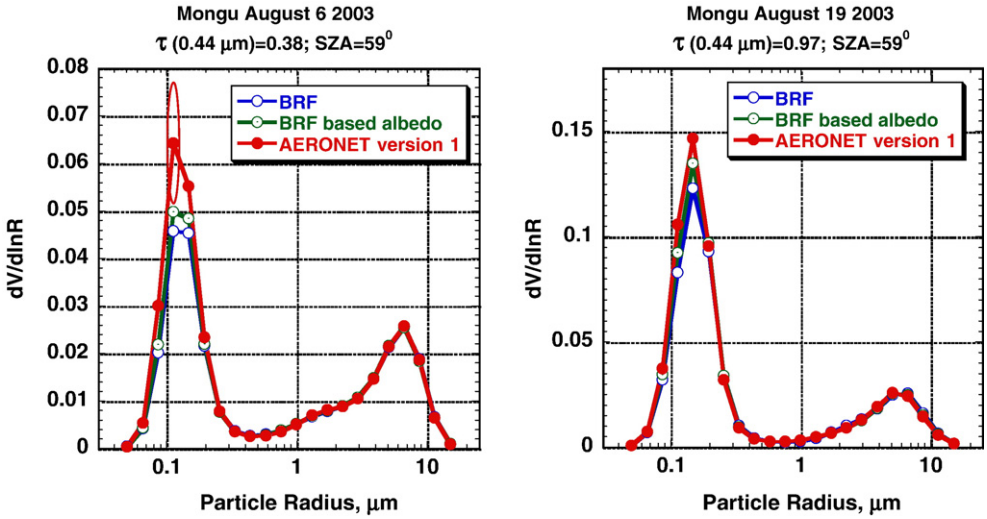

Fig. 17. Illustration of particle size distribution retrieval sensitivity to different assumed surface reflectivities at the Mongu AERONET site. The left and right panels present results for low and high aerosol loading, respectively. Error bars estimated in Dubovik et al. (2000) are depicted for the particle size distribution maximum in the left panel.

assumed that a 50% range in the prescribed ground albedo was sufficient to cover the uncertainty in natural surface reflectance variability. The analysis showed that for a Lambertian surface, this level of uncertainty does not substantially affect the accuracy of the retrieved aerosol parameters. Fig. 16 shows that the difference between the surface albedo assumed in the AERONET operational retrievals and of albedo produced by the joint inversion exceeds 50%, reaching ~100% and 500% for Mongu and Solar Village, respectively. This suggests that the effect of surface reflectance assumptions on AERONET aerosol retrievals should be reevaluated.

To assess the sensitivity of AERONET retrievals to surface reflectance uncertainty, the observations at Mongu and Solar Village sites were inverted with three different surface reflectance models: 1) anisotropic reflectance, using the BRF retrieved from the joint set of ground-based and satellite observations; 2) Lambertian reflectance, with surface albedo calculated from retrieved BRF; 3) Lambertian reflectance, with surface albedo assumed by version 1 of the AERONET operational aerosol retrieval algorithm. To avoid retrieval dependence on aerosol vertical distribution only almucantar measurements were used in the analysis. For each site, two sets of observations, having different aerosol loading conditions, were selected. The BRF retrieved from the joint observations were considered the true surface reflectance. Aerosol properties derived using retrieved BRF are then compared to aerosol retrievals obtained assuming surface reflectance models 2) and 3).

Figs. 17, 18, and 19 show the particle size distribution, real part of refractive index, and single scattering albedo respectively, retrieved at the Mongu site. Each figure has two panels presenting retrievals for low (left panel) and high (right panel) aerosol loading. As illustrated by Figs. 17 and 18, the surface reflectance underestimation (see Fig. 16) results in increased

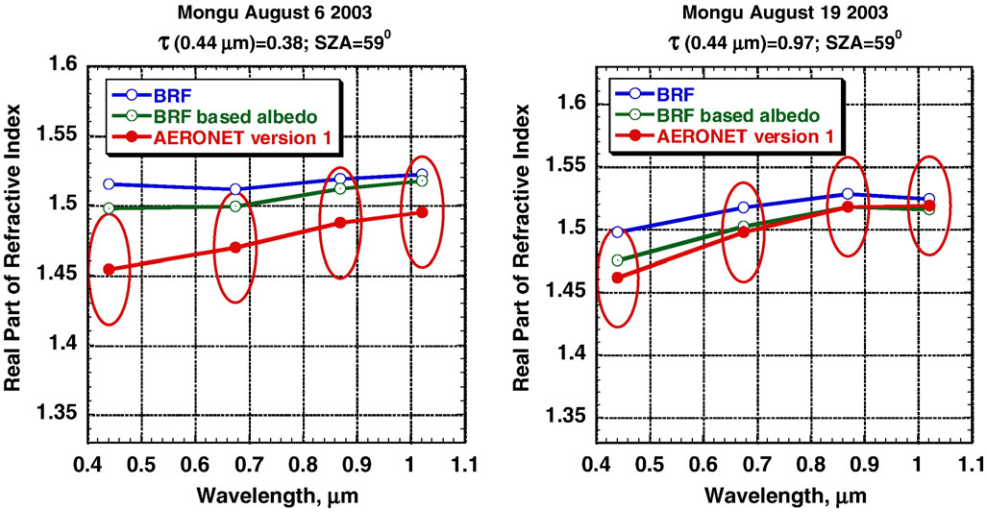

Fig. 18. The same as Fig. 17, but for the real part of the refractive index. Error bars for the version 1 AERONET operational algorithm are from Dubovik et al. (2000).

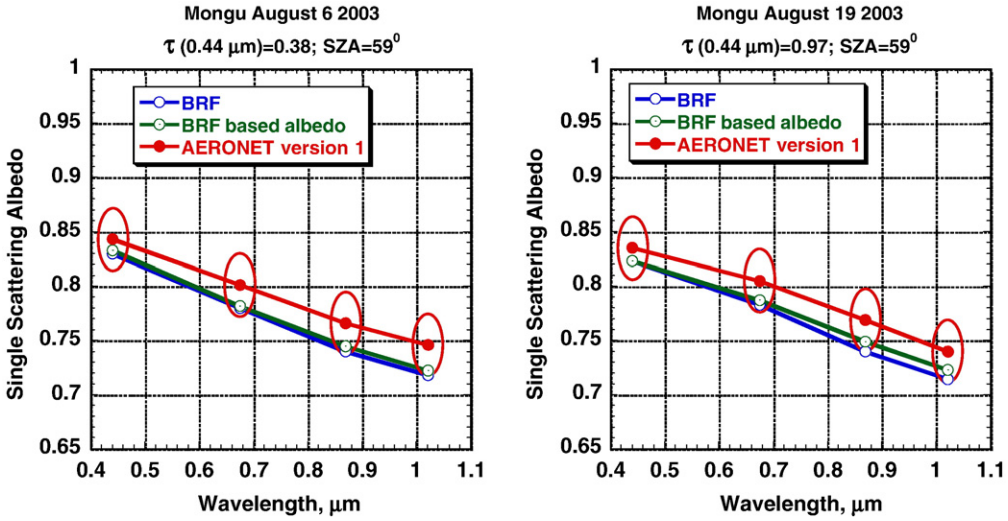

Fig. 19. The same as Fig. 18, but for single scattering albedo.

fine-mode particle concentration and an accompanying decrease in the real part of the refractive index. Apparently, the algorithm compensates for the lower surface reflectance contribution by increasing the contribution from the aerosols. The decrease in the real part of the refractive index, coincident with the increase of fine particle volume concentration, increases the aerosol phase function at large scattering angles without changing the aerosol optical depth (which is fixed by AERONET direct-sun observations). The prescribed surface reflectance uncertainty also decreases the imaginary part of the refractive index (not shown). All of the above tendencies create an increase in the retrieved values of single scattering albedo in the AERONET operational retrieval algorithm version 1, as illustrated in Fig. 19. It should be mentioned that the results of numerical tests performed separately (not shown) produced the same aerosol retrieval dependence on surface assumptions as presented above.

Both the left and right panels of Figs. 17–19 show close agreement between BRF based retrievals and retrievals based on the surface albedo obtained by angular integration of BRF. This means that at least for the same sun elevation, the Lambertian surface assumption constitutes a reasonable approximation for ground-based aerosol retrievals. However, using the same surface albedo for different sun elevations may not be sufficient because surface albedo varies as a function of solar zenith angle.

The errors in retrieved aerosol parameters due to surface model 3) (AERONET operational algorithm, version 1) depend on aerosol loading magnitude. As illustrated by the right panels of Figs. 17–19, the errors are smaller for higher aerosol optical depth, and lie within the error bars estimated by Dubovik et al. (2000) as a result of perturbation by random measurement errors, instrumental offsets and biases of the radiation model. The left panels of the same figures, showing low aerosol optical depth cases, demonstrate that uncertainties in retrievals of the

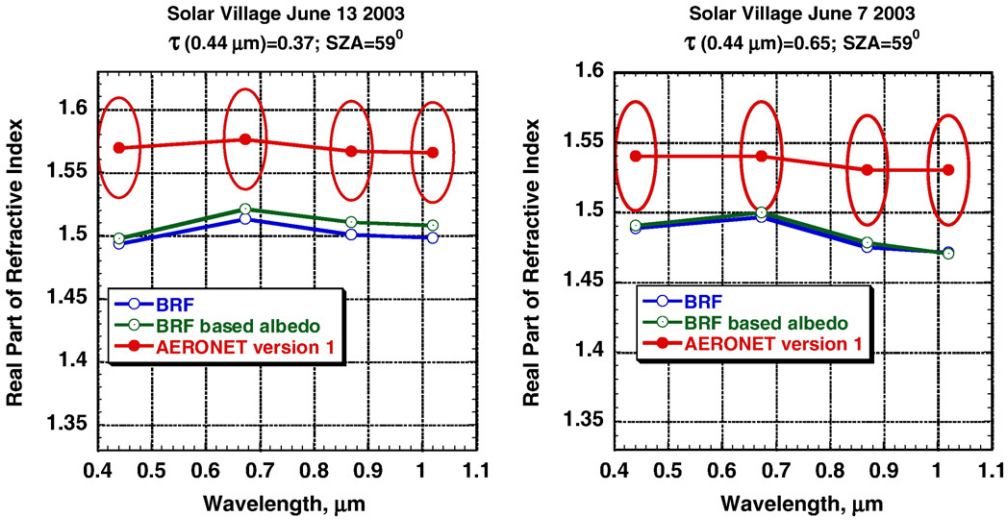

Fig. 20. The same as Fig. 18, but for Solar Village site.

particle size distribution maximum and retrievals of 0.44 μm real part of the refractive index exceed the error limits predicted by Dubovik et al. (2000). The retrieval results for single scattering albedo, however, are very similar for both low and high aerosol optical depth conditions (Fig. 19). This can be explained by the fact that opposing tendencies in the variation of particle concentration and the real part of the refractive index are partly compensating each other. In this case, the main factor affecting single scattering albedo is the reduction in the imaginary part of the refractive index, which is similar for low and high aerosol loading (~25% and ~20% on average for low and high aerosol loading, respectively). The above results suggest that the ground-based aerosol retrievals sensitivity to surface reflectance decreases with increasing aerosol loading.

Sensitivity study results for Solar Village are presented in Figs. 20 and 21 for the real part of the refractive index and single scattering albedo, respectively. Particle size distribution retrievals are not shown because they do not exhibit any substantial dependence on surface reflectance. As is seen from Figs. 20 and 21, aerosol retrieval dependence on surface assumptions are generally similar to those observed in the tests for the Mongu site (Figs. 17–19). Namely, the retrievals obtained with BRF and BRF-based surface albedo are in good agreement for both low and high aerosol loadings, and the effect of surface reflectance decreases with increased aerosol optical depth. The errors in aerosol parameters retrieved by using the AERONET operational version 1 surface model, however, are larger than in the Mongu case because the prescribed surface reflectance error is larger. For example, to compensate for surface albedo underestimation, it requires ~85% and 70% decrease in imaginary part of the refractive index (0.07 and 0.05 increase in real part of refractive index) at low and high aerosol loading, respectively. This produces larger errors in the retrieved real part of the refractive index than were estimated by Dubovik et al. (2000). This is also the case for single scattering albedo retrievals at low aerosol optical depth. However, as shown in the right panel of Fig. 21, increased aerosol loading brings the single scattering albedo retrieval errors for the long wave channels within the error bars of Dubovik et al. (2000).

5. Summary and conclusions

5.1. Retrieval method

A method for simultaneously retrieving aerosol and surface properties from a combination of ground-based and satellite observations was developed, taking advantage of complementary information from up- and down-looking observations of the same atmospheric column. This approach allows for a robust retrieval of both aerosol and surface properties.

The method retrieves particle size distribution, complex refractive index, and single scattering albedo along with bi-directional surface reflectance. Aerosol retrieval properties are parameterized in the same manner as in Dubovik and King (2000). Surface reflectance is modeled using the analytical RPV formulation (Rahman et al., 1993). The inversion is performed by a modified version of the AERONET retrieval algorithm, based on simultaneously fitting the entire data set of measurements and *a priori* constraints with a theoretical model (Dubovik & King, 2000).

The method was applied to combinations of AERONET measurements and observations from MISR, MODIS, and POLDER-2 satellite sensors over two AERONET sites: primarily smoke over Mongu, Zambia, and dust over Solar Village, Saudi Arabia. In all cases, the algorithm fit both ground-based and satellite observations by the theoretical model to the level of measurement accuracy (the values of residual were below 3–5%).

5.2. Surface retrievals

Applying the algorithm to AERONET data combined with observations by different satellite instruments (MODIS, MISR, and POLDER-2) produced relatively consistent surface property retrievals. Specifically, analyzing the retrieval results at

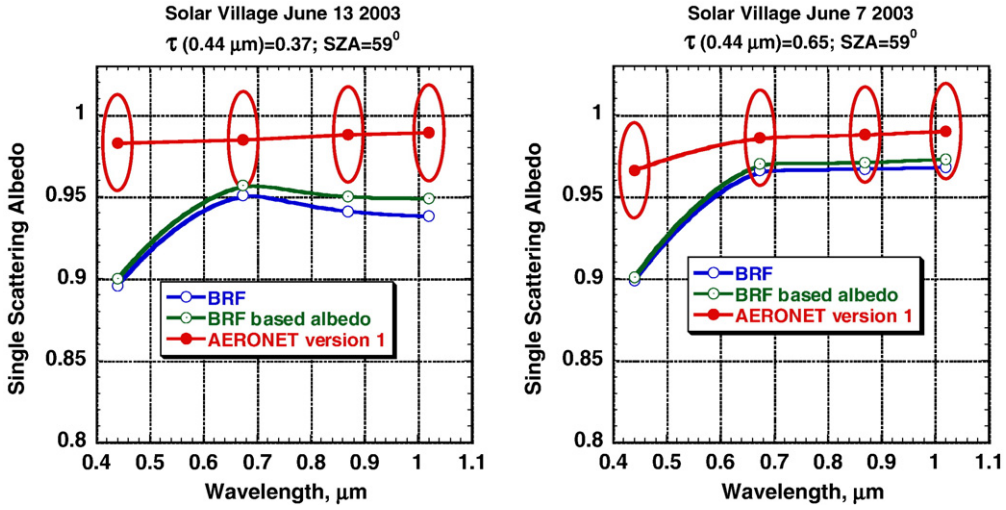

Fig. 21. The same as Fig. 19, but for Solar Village site.

Mongu and Solar Village, we found good agreement in both the angular and spectral characteristics of the retrieved BRF. A minor observed discrepancy between the MISR and POLDER-based retrievals in reflectance magnitude at longer wavelengths at Mongu was likely due to differences in satellite geo-location, spatial resolution, and angular sampling. To address the observational limitations of both the MISR and POLDER measurements over Solar Village (the observation planes are far from solar principal plane), spectral invariance of the BRF angular shape was employed as an additional constraint. Specifically, we imposed spectral smoothness constraints on the RPV model parameters responsible for the angular shape of BRF. This allowed us to improve the BRF and surface albedo retrievals at short wavelengths.

5.3. Testing algorithm robustness

The robustness of the algorithm was tested by analyzing time series of retrieved surface albedo for both selected AERONET sites during periods with no significant seasonal changes of surface reflectance and high variability of aerosol loading ($\tau(0.44) = \sim 0.2–1.0$ and $\sim 0.28–0.67$ at 0.44 μm for Mongu and Solar Village respectively). At Mongu, the retrievals at long wavelengths are very stable, having no significant temporal variability and no dependence on assumed aerosol vertical distribution. In contrast, retrievals at 0.44 μm showed dependence on the assumed aerosol profile, and exhibited temporal variability correlated with changes in aerosol optical depth. The correlation is small for low and moderate aerosol loading but increases significantly with an increase in aerosol optical depth above some boundary values between 0.65 and 0.85. This temporal variability could not be explained by a loss of surface reflectance sensitivity in the satellite observations, because the numerical simulations showed that a significant decrease in surface albedo retrieval accuracy occurs only for $\tau(0.44) \sim 1.5$ or higher. The analysis suggests that this correlation can be attributed to the combined effect of the errors in satellite radiometric calibration and uncertainty in aerosol vertical distribution.

Results of similar analysis for Solar Village showed that surface albedo retrievals at all the wavelengths exhibit some temporal variability that is not correlated with aerosol optical depth variability. This dependence can be explained by the difference in satellite angular sampling for different days. The surface retrievals at Solar Village did not exhibit substantial dependence on aerosol vertical distribution, as expected over the highly reflective desert surface. In addition, the range of aerosol optical depth was relatively small, which also reduces the expected influence of aerosol vertical distribution.

5.4. Sensitivity of surface retrievals to assumptions in the aerosol model

Surface retrieval sensitivity to the aerosol vertical distribution and aerosol particle shape assumptions was analyzed. The analysis showed that the assumption of aerosol vertical distribution affects the surface retrieval only at short wavelengths, where the error increases with increased aerosol loading. For example, surface albedo uncertainty due to an assumed aerosol profile retrieved at 0.44 μm reaches 0.035 for an aerosol optical depth ~ 0.85. However, for a value of aerosol optical depth ~ 0.7, the error was lower than 0.02. A similar tendency was found for the retrieved angular shape uncertainty in the shortwave BRF. We showed that desert dust aerosol non-sphericity significantly affects the angular shape of the retrieved BRF. For example, a transition from a bowl-like BRF shape for spheres to a bell-like BRF shape for spheroids was observed. At the same time, we found very weak retrieved surface albedo dependence on particle shape assumptions.

5.5. Sensitivity of AERONET aerosol retrievals to surface assumptions

From the joint inversion, the surface BRF retrieval results were used to reevaluate the AERONET operational aerosol retrieval uncertainty due to the assumed surface reflectance. The motivation for this was the fact that results of the surface BRF retrieval revealed higher uncertainty in AERONET surface assumptions then those used in sensitivity studies by (Dubovik et al., 2000). Also, the previous study did not consider the aerosol retrieval uncertainties caused by neglecting surface reflectance directionality. Our analysis showed that accounting for anisotropic surface reflectance is not critical for AERONET retrievals, whereas the error in surface reflectance magnitude may have a significant effect on retrieved aerosol properties. For example, the largest errors were encountered for the real part of the refractive index ($\sim 0.05–0.07$) retrievals, when the aerosol optical depth was small (~ 0.4 at 0.44 μm). The retrieved single scattering albedo uncertainties were within the error bars (0.03) estimated in Dubovik et al. (2000), with the exception of the 0.44 μm retrievals for the desert dust case. As expected, differences between the AERONET/satellite joint data retrieval and the AERONET operational aerosol retrieval (which relies on assumed surface properties) decreased with increasing aerosol loading.

Acknowledgments

We thank the EOS Project Science Office for continued support. We acknowledge support from NASA Radiation Sciences Program managed by Hal Maring. MISR data used in this study were obtained from the Atmospheric Sciences Data Center at NASA Langley Research Center.

References

Anderson, T. L., Masonis, S. J., Covert, D. S., Ahlquist, N. C., Howell, S. G., Clarke, A. D., et al. (2003). Variability of aerosol optical properties derived from in situ aircraft measurements during ACE—Asia. *Journal of Geophysical Research*, *108*, 8647. doi:10.1029/2002JD003247

Bruegge, C. J., Diner, D. J., Kahn, R., Chrien, N., Helmlinger, M. C., Gaitley, B. J., et al. (2006). The MISR radiometric calibration process. *Remote Sensing of Environment*, *107*, 2−11. doi:10.1016/j.rse.2006.07.024 (this issue).

Campbell, J. R., Welton, E. L., Spinhirne, J. D., Ji, Q., Tsay, S. C., Piketh, S. J., et al. (2003). Micropulse lidar observations of tropospheric aerosols over northeastern South Africa during the ARREX and SAFARI 2000 dry season

experiments. *Journal of Geophysical Research*, *108*. doi:10.1029/2002JD002563

Charlson, R. J., Schwartz, S. E., Hales, J. M., Cess, R. D., Coakley Jr., J. A., Hansen, J. E., et al. (1992). Climate forcing by anthropogenic aerosol. *Science*, *255*, 423–430.

Chin, M., Ginoux, P., Kinne, S., Torres, O., Holben, B. N., Duncan, B. N., et al. (2002). Tropospheric aerosol optical thickness from the GOCART model and comparisons with satellite and Sun photometer measurements. *Journal of the Atmospheric Sciences*, *59*, 461–483.

Deering, D. W., & Eck, T. F. (1987). Atmospheric optical depth effect on angular anisotropy of canopy reflectance. *International Journal of Remote Sensing*, *8*, 893–916.

Deering, D. W., Eck, T. F., & Banerjee, B. (1999). Characterization of the reflectance anisotropy of the boreal forest canopies in spring–summer. *Remote Sensing of Environment*, *67*, 205–229.

Deschamps, P. Y., Breon, F. M., Leroy, M., Podaire, A., Bricaud, A., Buries, J. C., et al. (1994). The POLDER mission: Instrument characteristics and scientific objectives. *IEEE Transactions on Geoscience and Remote Sensing*, *32*, 598–615.

Deuze, J. M., Breon, F. M., Devaux, C., Goloub, P., Herman, M., Lafrance, B., et al. (2001). Remote sensing of aerosols over land surfaces from POLDER-ADEOS-1 polarized measurements. *Journal of Geophysical Research*, *106*, 4913–4926.

Diner, D. J., Beckert, J. C., Reilly, T. H., Bruegge, C. J., Conel, J. E., Kahn, R. A., et al. (1998). Multi-angle Imaging SpectroRadiometer (MISR) instrument description and experiment overview. *IEEE Transactions on Geoscience and Remote Sensing*, *36*, 1072–1087.

Diner, D. J., Martonchik, J. V., Kahn, R. A., Pinty, B., Gobron, N., Nelson, D. L., et al. (2005). Using angular and spectral shape similarity constrains to improve MISR aerosol and surface retrievals over land. *Remote Sensing of Environment*, *94*, 155–171.

Dubovik, O. (2004). Optimization of numerical inversion in photopolarimetric remote sensing. In G. Videen, Y. Yatskiv, & M. Mishchenko (Eds.), *Photopolarimetry in remote sensing* (pp. 65–106). Dordecht, Netherlands: Kluwer Academic Publisher.

Dubovik, O., Holben, B., Eck, T. F., Smirnov, A., Kaufman, Y. J., King, M. D., et al. (2002). Variability of absorption and optical properties of key aerosol types observed in worldwide locations. *Journal of the Atmospheric Sciences*, *59*, 590–608.

Dubovik, O., Holben, B. N., Lapyonok, T., Sinyuk, A., Mishchenko, M. I., Yang, P., et al. (2003). Non-spherical aerosol retrieval method employing light scattering by spheroids. *Geophysical Research Letters*, *29*, 50-1–50-4.

Dubovik, O., & King, M. D. (2000). A flexible inversion algorithm for retrieval of aerosol optical properties from sun and sky radiance measurements. *Journal of Geophysical Research*, *105*, 20673–20696.

Dubovik, O., Sinyuk, A., Lapyonok, T., Holben, B., Mishchenko, M., Yang, P., et al. (2006). The application of spheroid models to account for the aerosol particle non-sphericity in remote sensing of desert dust. *Journal of Geophysical Research*, *111*, D11208. doi:10.1029/2005JD006619

Dubovik, O., Smirnov, A., Holben, B. N., King, M. D., Kaufman, Y. J., Eck, T. F., et al. (2000). Accuracy assessment of aerosol optical properties retrieved from AERONET sun and sky radiance measurements. *Journal of Geophysical Research*, *105*, 9791–9806.

Eck, T. F., Holben, B. N., Reid, J. S., Dubovik, O., Smirnov, A., O'Neill, N. T., et al. (1999). Wavelength dependence of the optical depth of biomass burning, urban, and desert dust aerosols. *Journal of Geophysical Research*, *104*, 31333–31349.

Ginoux, P., Chin, M., Tegen, I., Prospero, J. M., Holben, B., Dubovik, O., et al. (2001). Sources and distributions of dust aerosols simulated with the GOCART model. *Journal of Geophysical Research*, *106*, 20,255–20,273.

Goloub, P., Tanre, D., Deuze, J. L., Herman, M., Marchand, A., & Breon, F. M. (1999). Validation of the first algorithm applied deriving the aerosol properties over the ocean using POLDER/ADEOS measurements. *IEEE Transactions on Geoscience and Remote Sensing*, *37*, 1586–1596.

Gordon, H. R. (1997). Atmospheric correction of ocean color imaginary in the Earth Observing System era. *Journal of Geophysical Research*, *102*, 17,081–17,102.

Guenther, B., Xiong, X., Salomonson, V. V., Barnes, W. L., & Young, J. (2002). On-orbit performance of the Earth Observing System Moderate Resolution Imaging Spectroradiometer: First year of data. *Remote Sensing of Environment*, *83*, 16–30.

Hansen, J. M., Sato, M., & Ruedy, R. (1997). Radiative forcing and climate response. *Journal of Geophysical Research*, *102*, 6831–6864.

Hansen, J. M., Sato, M., Ruedy, R., Lacis, A., & Oinas, V. (2000). Global warming in the twenty-first century: An alternative scenario. *Proceedings of the National Academy of Sciences of the United States of America*, *97*, 9875–9880.

Haywood, J. M., Osborne, S. R., Francis, P. N., Keil, A., Formenti, P., Andreae, M. O., et al. (2003). The mean physical and optical properties of regional haze, dominated by biomass burning aerosols measured from the C-130 aircraft during SAFARI 2000. *Journal of Geophysical Research*, *108*, 8473.

Herman, M., Deuze, J. L., Marchand, A., Roger, B., & Lallart, P. (2005). Aerosol remote sensing from POLDER//ADEOS over the ocean: Improved retrieval using a non-spherical particle model. *Journal of Geophysical Research*, *110*, D10S02. doi:10.1029/2004JD004798

Henyey, L. G., & Greenstein, T. L. (1941). Diffuse radiation in the galaxy. *Astrophysics Journal*, *93*, 70–78.

Holben, B. N., Eck, T. F., Slutsker, I., Tanre, D., Buis, J. P., Setzer, A., et al. (1998). AERONET—A federated instrument network and data archive for aerosol characterization. *Remote Sensing of Environment*, *66*(1), 1–16.

Holben, B. N., Tanre, D., Smirnov, A., Eck, T. F., Slutsker, I., Abuhassan, N., et al. (2001). An emerging ground-based aerosol climatology: Aerosol optical depth from AERONET. *Journal of Geophysical Research*, *106*, 12067–12097.

Hsu, N. C., Tsay, S. C., King, M. D., & Herman, J. R. (2004). Aerosol properties over bright-reflecting source regions. *IEEE Transactions on Geoscience and Remote Sensing*, *42*, 557–569.

Intergovernmental Panel on Climate Change (IPCC) (2001). In J. H. Houghton (Ed.), *Climate change 2001: The scientific basis* New York: Cambridge Univ. Press 881 pp.

Irons, J. R., Campbell, G. S., Norman, J. M., Graham, D. W., & Kovalick, W. M. (1992). Prediction and measurements of soil bidirectional reflectance. *IEEE Transactions on Geoscience and Remote Sensing*, *30*, 249–260.

Kalashnikova, O. V., Kahn, R., Sokolik, I. N., & Li, W. H. (2005). Ability of multiangle remote sensing observations to identify and distinguish mineral dust types: Optical models and retrievals of optically thick plumes. *Journal of Geophysical Research*, *110*, D18 (Art. No. D18S14).

Kalashnikova, O. V., & Sokolik, I. N. (2002). Importance of shapes and compositions of wind-blown dust particles for remote sensing at solar wavelengths. *Geophysical Research Letters*, *29* (Art. No. 1398).

Kahn, R., Banerjee, P., & McDonald, D. (2001). The sensitivity of multiangle imaging to natural mixtures of aerosols over ocean. *Journal of Geophysical Research*, *106*, 18219–18238.

Kahn, R. A., Gaitley, B. J., Martonchik, J. V., Diner, D. J., & Crean, K. A. (2005). Multiangle Imaging Spectroradiometer (MISR) global aerosol optical depth validation based on 2 years of coincident Aerosol Robotic Network (AERONET) observations. *Journal of Geophysics*, *110*. doi:10.1029/2004JD004706

Kaufman, Y. J., Gobron, N., Pinty, B., Wildowski, J. L., & Verstraete, M. M. (2002). Relationship between surface reflectance in the visible and mid-infrared used in MODIS aerosol algorithm: Theory. *Geophysical Research Letters*, *29*. doi:10.1029/2003JD003981

Kaufman, Y. I., & Sendra, C. (1988). Algorithm for atmospheric correction. *International Journal of Remote Sensing*, *9*, 1357–1381.

Kaufman, Y. J., Tanre, D., & Boucher, O. (2002). A satellite view of aerosol in the climate system. *Nature*, *419*, 215–223.

Kaufman, Y. J., Tanre, D., Remer, L. A., Vermote, E. F., Chu, A., & Holben, B. N. (1997). Operational remote sensing of tropospheric aerosol over land from EOS moderate resolution imaging spectroradiometer. *Journal of Geophysical Research*, *102*, 17051–17068.

Kaufman, Y. J., Wald, A. E., Remer, L. A., Gao, B. C., Li, R. R., & Flynn, L. (1997). The MODIS 2.1-μm channel-correlation with visible reflectance for use in remote sensing of aerosol. *IEEE Transactions on Geoscience and Remote Sensing*, *35*, 1286–1298.

King, M. D., Kaufman, Y. J., Menzel, W. P., & Tanre, D. (1992). Remote sensing of cloud, aerosol and water vapor properties from moderate resolution imaging spectrometer (MODIS). *IEEE Transactions on Geoscience and Remote Sensing*, *30*, 2–27.

King, M. D., Kaufman, Y. J., Tanre, D., & Nakajima, T. (1999). Remote sensing of tropospheric aerosols from space: Past, present, and future. *Bulletin of the American Meteorological Society*, *80*, 2229−2259.

Kotchenova, S. Y., Vermote, E. F., Matarrese, R., & Klemm, F. (2006). Validation of a new vector version of the 6S radiative transfer code for atmospheric correction of MODIS data: Part I—Path radiance. *Applied Optics*, *45*, 6762−6774.

Lacis, A. A., Chowdhary, J., Mishchenko, M. I., & Cairns, B. (1998). Modeling errors in diffuse-sky radiation: Vector vs. scalar treatment. *Geophysical Research Letters*, *25*, 135−138.

Lucht, W., & Roujean, J. L. (2000). Consideration in parametric modeling of BRDF and albedo from multi-angular satellite sensors observations. *Remote Sensing Reviews*, *18*, 343−379.

Lyapustin, A., Martonchik, J., Privette, J., Holben, B., Slutsker, I, Sinyuk, A., et al. (2006). Local analysis of MISR surface BRF and albedo over GSFC and Mongu AERONET sites. *IEEE Transactions on Geoscience and Remote Sensing*, *44*, 1707−1718.

Maignan, F., Breon, F. M., & Lacaze, R. (2004). Bidirectional reflectance of Earth targets: Evaluation of analytical models using a large set of space-borne measurements with emphasis on Hot-Spot. *Remote Sensing of Environment*, *9*, 210−220.

Martonchik, J. V., Diner, D. J., Kahn, R., Verstraete, M. M., Pinty, B., Gordon, H. R., et al. (1998). Techniques for the retrieval of aerosol properties over land and ocean using multiangle imaging. *IEEE Transactions on Geoscience and Remote Sensing*, *36*, 1212−1227.

McGill, M. J., Hlavka, D. L., Hart, W. D., Welton, E. J., & Campbell, J. R. (2003). Airborne lidar measurements of aerosol optical properties during SAFARI-2000. *Journal of Geophysical Research*, *108*. doi:10.1029/2002JD002370

Minnaert, M. (1941). The reciprocity principle in lunar photometry. *Astrophysics Journal*, *93*, 403−410.

Mishchenko, M. I., Cairns, B., Hansen, J. E., Travis, L. D., Burg, R., Kaufman, Y. J., et al. (2004). Monitoring of aerosol forcing of climate from space: Analysis of measurement requirements. *Journal of Quantitative Spectroscopy & Radiative Transfer*, *88*, 149−161.

Mishchenko, M. I., Lacis, A. A., & Travis, L. D. (1994). Errors induced by the neglect of polarization in radiance calculations for Rayleigh-scattering atmospheres. *Journal of Quantitative Spectroscopy & Radiative Transfer*, *51*, 491−510.

Mishchenko, M. I., Travis, L. D., & Kahn, R. A. (1997). Modeling phase function of dustlike tropospheric aerosols using a shape mixture of randomly oriented polydisperse spheroids. *Journal of Geophysical Research*, *102*, 16831−16847.

Mishchenko, M. I., Travis, L. D., & Lacis, A. A. (2002). *Scattering, absorption, and emission of light by small particles.* Cambridge: Cambridge Univ. Press.

Nakajima, T., & Tanaka, M. (1986). Matrix formulation for the transfer of solar radiation in plane-parallel scattering atmosphere. *Journal of Quantitative Spectroscopy & Radiative Transfer*, *35*, 13−21.

Nakajima, T., & Tanaka, M. (1988). Algorithms for radiative intensity calculations in moderately thick atmosphere using a truncation approximation. *Journal of Quantitative Spectroscopy & Radiative Transfer*, *40*, 51−69.

Pinty, B., Lattanzio, A., Martonchik, J. V., Verstraete, M. M., Gobron, N., Taberner, M., et al. (2005). Coupling diffuse sky radiation and surface albedo. *Journal of the Atmospheric Sciences*, *62*, 2580−2591.

Privette, J. L., Eck, T. F., & Deering, D. W. (1997). Estimating spectral albedo and nadir reflectance through inverting simple BRDF models with AVHRR/MODIS like data. *Journal of Geophysical Research*, *102*, 29529−29542.

Quijano, A. L., Sokolik, I. N., & Toon, O. B. (2000). Influence of aerosol vertical distribution on the retrievals of aerosol optical depth from satellite radiance measurements. *Geophysical Research Letters*, *27*, 3457−3460.

Rahman, H., Pinty, B., & Verstraete, M. M. (1993). Coupled surface–atmosphere reflectance (CSAR) model 2.Semi-empirical surface model usable with NOAA Advanced Very High Resolution Radiometer data. *Journal of Geophysical Research*, *98*, 20,791−20,801.

Ramanathan, V., Crutzen, P. J., Lelieveld, J., Mitra, A. P., Althausen, D., Anderson, J., et al. (2001). Indian Ocean experiment: An integrated analysis of the climate forcing and effects of the great Indo-Asian haze. *Journal of Geophysical Research*, *106*, 28,371−28,398.

Reid, J. S., Hobbs, P. V., Ferek, R. J., Blake, D. R., Martins, J. V., Dunlap, M. R., et al. (1998). Physical, chemical, and optical properties of regional hazes dominated by smoke in Brazil. *Journal of Geophysical Research*, *103*, 32059−32080.

Remer, L. A., Kaufman, Y. J., Tanre, D., Mattoo, S., Chu, D. A., Martins, J. V., et al. (2005). The MODIS Aerosol algorithm, products, and validation. *Journal of the Atmospheric Sciences*, *62*, 947−973.

Remer, L. A., Tanre, D., Kaufman, Y. J., Ichoku, C., Mattoo, S., Levy, R., et al. (2002). Validation of MODIS aerosol retrieval over ocean. *Geophysical Research Letters*, *29*, 12. doi:10.1029/2001GL013204

Roberts, G. (2001). A review of the application of BRDF models to infer land cover parameters at regional and global scales. *Progress in Physical Geography*, *25*, 483−511.

Schaaf, C. B., Gao, F., Strahler, A. H., Lucht, W., Li, X., Tsang, T., et al. (2002). First operational BRDF, albedo nadir reflectance products from MODIS. *Remote Sensing of Environment*, *83*, 135−148.

Sellers, P. J. (1993). *Remote sensing of the land surface for studies of global change, NASA/GSFC.* Int. Satell. Land Surface Climatol. Proj. Rep., Columbia, Md.

Sinyuk, A., Torres, O., & Dubovik, O. (2003). Combined use of satellite and surface observations to infer the imaginary part of refractive index of Saharan dust. *Geophysical Research Letters*, *30*, 1081. doi:10.1029/2002GL016189

Smirnov, A., Holben, B. N., Dubovik, O., & Slutsker, I. (2000). Cloud screening and quality control algorithms for the AERONET data base. *Remote Sensing of Environment*, *73*, 73 337−73 349.

Tanre, D., Kaufman, Y. Y., Herman, M., & Mattoo, S. (1997). Remote sensing of aerosol properties over ocean using the MODIS/EOS spectral radiances. *Journal of Geophysical Research*, *102*, 16971−16988.

Tegen, I., Hollrig, P., Chin, M., Fung, I., Jacob, D., & Penner, J. (1997). Contribution of different aerosol species to the global aerosol extinction optical thickness: Estimates from model results. *Journal of Geophysical Research*, *102*, 23,895−23,915.

Tegen, I., Lacis, A. A., & Fung, I. (1996). The influence of climate forcing of mineral aerosol from disturbed soils. *Nature*, *380*, 419−422.Tegen, I., Lacis, A. A., & Fung, I. (1996). The influence of climate forcing of mineral aerosol from disturbed soils. *Journal of Geophysical Research*, *102*, 16971−16988.

Torres, O., Bhartia, P. K., Herman, J. R., Ahmad, Z., & Gleason, J. (1998). Derivation of aerosol properties from satellite measurements of back-scattered ultraviolet radiation: Theoretical basis. *Journal of Geophysical Research*, *103*, 17099−17110.

Torres, O., Bhartia, P. K., Sinyuk, A., Welton, E. J., & Holben, B. (2005). Total Ozone Mapping Spectrometer measurements of aerosol absorption from space: Comparison to SAFARI 2000 ground-based observations. *Journal of Geophysical Research*, *110*. doi:10.1029/2004JD004611

Volten, H., Muñoz, O., Rol, E., de Haan, J. F., Vassen, W., Hovenier, J. W., et al. (2001). Scattering matrices of mineral particles at 441.6 nm and 632.8 nm. *Journal of Geophysical Research*, *106*, 17375−17401.